

NASA Contractor Report 185192

Unified Aeroacoustics Analysis for High Speed Turboprop Aerodynamics and Noise

Volume II - Development of Theory for Wing Shielding

R. K. Amiet
*United Technologies Research Center
East Hartford, Connecticut*

May 1991

Prepared for
Lewis Research Center
Under Contract Number NAS3-23720



National Aeronautics and
Space Administration

(NASA-CR-185192) UNIFIED AEROACOUSTICS
ANALYSIS FOR HIGH SPEED TURBOPROP
AERODYNAMICS AND NOISE. VOLUME 2:
DEVELOPMENT OF THEORY FOR WING SHIELDING
Final Report (United Technologies Research 63/71

N91-23849
Unclas
001365o



NASA Contractor Report 185192

Unified Aeroacoustics Analysis for High Speed Turboprop Aerodynamics and Noise

Volume II - Development of Theory for Wing Shielding

R. K. Amiet
United Technologies Research Center
East Hartford, Connecticut

May 1991

Prepared for
Lewis Research Center
Under Contract Number NAS3-23720



National Aeronautics and
Space Administration



TABLE OF CONTENTS

Summary	1
Introduction	2
Analysis	3
A. Zero Mean Flow	3
1. Exact solution	3
2. Integral approximation	4
B. With Mean Flow	5
1. Unswept wing	5
2. Swept wing	7
3. Leading and trailing edge cases	7
4. Normalization of the solution	8
Comparison with Other Solutions	12
Behavior of the Solution	13
The Computer Programs	14
Conclusions	15
References	15
List of Symbols	16
Appendix A: Main Program for Calculating Diffraction by an Edge	17
Appendix B: Subroutine for Calculation of Integral in Equation (8)	19
Appendix C: Subroutine for Calculation of R, S, μR and μS	20
Appendix D: Subroutine for Transforming Sweep and Flow	21
Appendix E: Subroutine for Simpson's Rule Integration	22
Appendix F: Subroutine for Evaluation of Fresnel Integrals	23
Appendix G: Subroutine for Calculation of Integrand in Equation (8)	24
Appendix H: Subroutine for Calculation of the Bessel Functions	25
Appendix I: Subroutine for Calling the Subroutine INTH	26
Appendix J: Subroutine for Calculating a Power Series	27
Figures	28-37

1
2
3
4
5
6
7
8
9
10
11
12
13
14
15
16
17
18
19
20
21
22
23
24
25
26
27
28
29
30
31
32
33
34
35
36
37
38
39
40
41
42
43
44
45
46
47
48
49
50
51
52
53
54
55
56
57
58
59
60
61
62
63
64
65
66
67
68
69
70
71
72
73
74
75
76
77
78
79
80
81
82
83
84
85
86
87
88
89
90
91
92
93
94
95
96
97
98
99
100

Diffraction of Sound by a Half-Plane in a Uniform Flow

R. K. Amiet

SUMMARY

The classical problem of the diffraction of sound by a half-plane is extended to the case where the half-plane is immersed in a uniform flow. Both the leading edge and trailing edge cases are considered. The sound source is assumed to be a point source. Computer programs are presented for the evaluation of the necessary integrals. The results are expressed relative to both the sound that would be present in the absence of the half-plane and the sound at the point on the edge where the ray passes the edge. A minor misrepresentation of the solution in the literature has been clarified for the case $\tau_k > 0$, which corresponds to the illuminated region. Several sample calculations are presented.

INTRODUCTION

This document is Volume II of a 5 volume report on aerodynamics and noise of advanced turboprops. Volumes I, III and IV relate to aerodynamic and acoustic disturbances caused by the blades and Volume V relates to shielding of propeller noise in the cabin by the fuselage boundary layer. This volume presents theory and a computer code developed for evaluation of the shielding benefit that might be expected by an airplane wing in a wing-mounted propeller installation. Several computed directivity patterns are presented to demonstrate the theory. Application to actual airplane geometry is given in Volume III.

The diffraction of a sound or electromagnetic wave by a half-plane is a classic problem in the literature. The first rigorous solution for the case of a plane wave incident on a half-plane was given by Sommerfeld (ref. 1). Other authors (refs. 2-6) have subsequently treated this problem. This fundamental solution has been extended by many authors to other cases such as the diffraction of a point source field by a half-plane, the diffraction of a plane wave by a wedge, the case where the half-plane is considered "soft" (the boundary condition of no-flow through the surface is replaced by some other boundary condition), etc.

The primary interest of these solutions has been for electromagnetic applications, with acoustics being a secondary interest. For the electromagnetic problem there is no such thing as a mean flow, so the case of diffraction in a flow has received little attention. Thus, it has only been recently with the advent of the concept of using the wing of an aircraft for noise shielding that the case of diffraction by a surface in a flow has been given attention.

The present analysis is based on the case of diffraction with no flow. By combining a Galilean and a Lorentz transform, the wave equation with a mean flow can be reduced to the ordinary wave equation. The boundary conditions must also be transformed, but because of the simple geometry of the problem the boundary conditions remain unchanged in the transformed plane. A similar transformation was used by Candel (ref. 7).

Allowance is also made in the analysis for the case of a swept wing. The same combination of Galilean and a Lorentz transforms mentioned above lead to a problem with no flow but a different sweep. Thus, with proper interpretation and reverse transformation of the zero flow case, one can obtain the solution for the effect of sweep. This is included in the computer program.

The solution procedures for the cases of leading and trailing edges are basically the same. For the leading edge one works with the velocity potential since the boundary condition is on normal velocity. For the trailing edge the boundary condition in the wake is that there be no pressure jump. For this case the same solution applies, but the fundamental variable is the pressure.

Two normalizations of the solution are given by the computer program. The first is just to normalize the solution by the pressure that would exist at the observer in the absence of the plate. The second choice is to normalize the solution by the pressure at the point on the edge at which the ray crosses in passing to the observer. This edge pressure calculated in the absence of the plate is extrapolated to be an equal distance from the source as the observer. The reason for this second normalization is to better represent those cases where the point source is very directional. The pressure at the observer in the absence of the plate bears no relation to the diffracted field at the observer in the presence of the plate, whereas the pressure at the edge crossing point is on the ray that moves from the source to the observer.

FORTRAN computer programs are presented with detailed documentation. The output from these programs compares favorably with the results of other investigators.

ANALYSIS

A. Zero Mean Flow

1. Exact solution

The solution for the sound field of a source near a semi-infinite plane without flow has been given previously (refs. 1 - 6) so that here all that need be done is to give a summary of the results. The geometry of the problem is shown in figure 1. Mathematically the problem can be stated as follows.

A source of strength $Q_0 \exp(i\omega t)$ at (x_0, y_0, z_0) induces a velocity potential Φ_0 that satisfies the wave equation

$$(\nabla^2 + k^2) \Phi_0 = Q_0 \delta(x - x_0) \delta(y - y_0) \delta(z - z_0) \quad (1)$$

where $k = \omega/c_0$. The plate is assumed to lie in the $y = 0$ plane in the region $x > 0$. The boundary condition of no flow through the plate is

$$v_y = \partial \Phi_0 / \partial y = 0 \quad \text{on } y = 0, x > 0 \quad (2)$$

The solution to this problem can be written (ref. 4)

$$\Phi_0 = Q_0 \frac{ik}{8\pi} \left[\int_{-\mu_R}^{\infty} H_1^{(2)}(kR \cosh \mu) d\mu + \int_{-\mu_S}^{\infty} H_1^{(2)}(kS \cosh \mu) d\mu \right] \quad (3)$$

where

$$R \equiv \sqrt{r_o^2 + r_s^2 - 2r_o r_s \cos(\theta_o - \theta_s) + (z_o - z_s)^2} \quad S \equiv \sqrt{r_o^2 + r_s^2 - 2r_o r_s \cos(\theta_o + \theta_s) + (z_o - z_s)^2}$$

$$\mu_R \equiv \sinh^{-1} \left[\frac{2}{R} \sqrt{r_o r_s} \cos \left(\frac{\theta_o - \theta_s}{2} \right) \right] \quad \mu_S \equiv \sinh^{-1} \left[\frac{2}{S} \sqrt{r_o r_s} \cos \left(\frac{\theta_o + \theta_s}{2} \right) \right]$$

The source coordinates are $\mathbf{x}_s = (x_s, y_s, z_s)$ (or (r_s, θ_s, z_s) in polar coordinates) and the observer coordinates are $\mathbf{x}_o = (x_o, y_o, z_o)$ or (r_o, θ_o, z_o) .

As a check on the solution, consider placing the observation point near the source; i.e., $\mathbf{x}_o \rightarrow \mathbf{x}_s$. Then $R \rightarrow 0$ and $\mu_R \rightarrow \infty$. The second integral in equation (3) remains bounded while the first goes to infinity as R^{-1} . Because of the factor R in the argument of the Hankel function, it is not immediately obvious that the upper limit μ_R of the integral can be set equal to infinity in the $R \rightarrow 0$ limit. It can be shown, however, that the major contribution to the integral comes from the region $\mu \approx 0$; using the relation

$$-\frac{i}{2} \int_{-\infty}^{\infty} H_1^{(2)}(a \cosh \mu) d\mu = \frac{1}{a} e^{-ia} \quad (4)$$

(see Born and Wolf (ref. 6, p.586)) equation (3) becomes

$$\Phi_0 \rightarrow -Q_0/(4\pi R) + O(1) \quad \text{as } R \rightarrow 0 \quad (5)$$

Then, near the source, $v_R = \partial \Phi_0 / \partial R = Q_0/(4\pi R^2)$. Considering a small sphere around the source and multiplying the velocity by the area $4\pi R^2$, the total volume flow out of the sphere is found to be Q_0 . Thus, equation (3) represents the diffraction field of a monopole source of strength Q_0 near a half plane. This is consistent with equation (1), the right hand side of which can be shown to represent a monopole.

2. Integral approximations

The integrals in equation (3) can be approximated for large k . The two integrals are similar in form so that only the approximation for the first will be discussed. This integral will be analyzed in the two regimes $\mu_R > 0$ and $\mu_R < 0$. For $\mu_R < 0$ both limits on the integral are positive. For $\mu_R > 0$, the integral will first be divided into two integrals; one with limits $\pm\infty$ and one with both limits negative; the integral with infinite limits can be evaluated in closed form, and the integral with both limits negative is treated in the same way as for the case when both limits are positive.

Thus, first consider the case $\mu_R < 0$ for which both limits are positive. It follows from the definitions of μ_R and R in equation (3) that

$$R \cosh \mu_R = \sqrt{(r_o + r_s)^2 + (z_o - z_s)^2} \equiv R_1 \quad (6)$$

Thus, over the entire range of integration (for which $\mu > |\mu_R|$) the following inequality holds:

$$kr \cosh \mu \geq kR_1 \quad (7)$$

For $kR_1 \gg 1$ the Hankel function can be replaced by its asymptotic form for large argument giving

$$\begin{aligned} I &\equiv \int_{-\mu_R}^{\infty} H_1^{(2)}(kr \cosh \mu) d\mu \approx -\sqrt{\frac{2}{\pi kR}} e^{-i\pi/4} \int_{-\mu_R}^{\infty} e^{-ikR \cosh \mu} \frac{d\mu}{\sqrt{\cosh \mu}} \\ &= -2\sqrt{\frac{2}{\pi kR}} e^{-i(kR + \pi/4)} \int_{-\tau_R}^{\infty} \frac{e^{-ikR \tau^2}}{\sqrt{(\tau^2 + 1)(\tau^2 + 2)}} d\tau \end{aligned} \quad (8)$$

where the parameter τ , defined as

$$\tau = \sqrt{2} \sinh(\mu/2) \quad (9)$$

was introduced in place of μ . The definition of μ_R from equation (3) gives for the corresponding value of τ_R

$$\tau_R = 2 \sqrt{\frac{r_o r_s}{R(R + R_1)}} \cos\left(\frac{\theta_o - \theta_s}{2}\right) = \begin{cases} \sqrt{R_1/R - 1} & \theta_o - \theta_s \leq \pi \\ -\sqrt{R_1/R - 1} & \theta_o - \theta_s \geq \pi \end{cases} \quad (10)$$

Equation (8) can be approximated further. Since kR is large, variation with μ of the exponent $kR \cosh \mu$ is also large, and the method of stationary phase can be used to evaluate the integral. Since the derivative of the phase is zero only at the point $\mu = 0$ and since this point is not included within the range of integration, there are no stationary phase points. Following Senior (ref. 4), τ is set equal to its lower limit in the non exponential part of the integral. The justification for this can be found in the book by Erdelyi (ref. 8), p.51, under a discussion of the method of stationary phase. For integrals with rapidly varying phase the major contribution comes from the end points and any stationary phase points. Because the portion of the integrand under the radical in equation (8) varies slowly compared to the phase of the exponential, it is justifiable to set the argument under the radical equal to the constant value taken at the end point of the integration. Substitution from equation (10) in equation (8) gives the approximate value valid for large kR_1

$$I \approx -\frac{2}{kR} e^{-i(kR + \pi/4)} \frac{R}{\sqrt{R_1(R_1 + R)}} F^*(-\tau_R \sqrt{2kR/\pi}) \quad \tau_R < 0 \quad (11)$$

where

$$F^*(x) \equiv \int_x^{\infty} e^{-it^2 \pi/2} dt \quad (12a)$$

F^* is related to the Fresnel integrals $C(x)$ and $S(x)$ by

$$F^*(x) = \frac{1-i}{2} - E^*(x) \quad (12b)$$

where

$$E^*(x) \equiv C(x) - i S(x) = \int_0^x e^{i^2 \pi t} dt \quad (12c)$$

Equation (11) is valid only for $\tau_R < 0$. The case $\tau_R > 0$ is treated simply by dividing the integration range into two parts as discussed previously. The integral with limits $\pm \infty$ is found in closed form using equation (4). The integral with both limits negative is treated in the same manner as for positive limits, and is easily found to give the same result. The final result for $\tau_R > 0$ is

$$I \approx e^{-ikR} \frac{2}{kR} \left[i + e^{-i\pi/4} \frac{R}{\sqrt{R_1(R_1 + R)}} F^*(\tau_R \sqrt{2kR/\pi}) \right] \quad \tau_R > 0 \quad (13)$$

For $\tau_R = 0$ Eqs. (11) and (13) become identical. The first term in equation (13) is the field of a source in free space, while the second gives the contribution of the edge. For a physical interpretation of the difference between Eqs. (11) and (13), note that from equation (10) for $\theta_o - \theta_s < \pi$ that equation (13) applies when $\theta_o - \theta_s < \pi$; i.e., when the observer is not in the shadow of the plate, while equation (11) is for an observer in the shadow. For the second term in equation (3), an equation similar to equation (13) applies for an observer that can see the reflection of the source in the plate ($\theta_o + \theta_s < \pi$), and an equation similar to equation (11) applies for an observer who cannot ($\theta_o + \theta_s > \pi$).

The author has not found in the literature the two different forms which were given here for the two regions $\tau_R > 0$ and $\tau_R < 0$. Thus, Senior (ref. 4, eq. (33)) and Born and Wolf (ref. 6, eq. (45) of section 11.7) give the same result as equation (11) here, but do not make a distinction for the case $\tau_R > 0$. In Eqs. (11) and (13) above, the function F^* always has a positive argument. The results given by Senior and by Born and Wolf have a negative argument for F^* when $\tau_R > 0$; this can be rewritten with a positive argument by dividing the range in the integration of F^* in equation (12a) into two ranges, one with limits $\pm \infty$ and the other with both limits negative (which is the same as both limits positive). The function F^* will then be the same as in equation (13) above, but the integrated part will have a factor $R/[R_1(R_1 + R)/2]^{1/2}$ that does not appear in equation (13). This may not have been noticed earlier since for positive τ_R the discrepancy between equation (11) and equation (13) is most apparent in the illuminated region where the diffraction effects are minimal and so not of interest to calculate. Near the diffraction zone $\tau_R = 0$ and Eq. (10) shows that $R_1 \sim R$ so that the factor $R/[R_1(R_1 + R)/2]^{1/2}$ is nearly equal to 1.

Both the exact and the approximate solutions are antisymmetrical about $\mu_R = \tau_R = 0$. Thus, only the region $\tau_R < 0$ need be considered in detail. If the results are plotted against the variable $\tau_R (kR)^{1/2}$ then the argument of F^* in equation (11) is given by the abscissa. If the integral is multiplied by the factors appearing before F^* in equation (11), the asymptotic form of the integral will be independent of kR when plotted; the deviation of the exact solution from this approximate curve will then show more clearly than if I in Eqs. (8) and (11) is plotted directly. This plot given in figure 2 clearly shows that for values of $kR > 1$ the approximate result is very close to the exact integral.

B. With Mean Flow

1. Unswept wing

The addition of a mean flow to the problem will now be considered. Without flow, and for a general time dependence the problem can be formulated in terms of the velocity potential ϕ' as the following boundary value problem:

$$\left(\nabla^2 - \frac{1}{c_0^2} \frac{\partial^2}{\partial t^2} \right) \phi' = Q(t) \delta(x - x_s) \delta(y - y_s) \delta(z - z_s) \quad (14)$$

The boundary conditions are

$$\partial \phi' / \partial y = 0 \quad \text{on } y = 0, x > 0 \quad (15)$$

For the problem with flow the edge of the plate will be assumed to be a leading edge, as opposed to a trailing edge which will be discussed later. The coordinate system is fixed to the plate with the source being stationary and the fluid moving toward increasing x ; see figure 1. The equation for the velocity potential ϕ becomes

$$\left[\nabla^2 - \left(\frac{1}{c_0} \frac{\partial}{\partial t} + M \frac{\partial}{\partial x} \right)^2 \right] \phi = Q(t) \delta(x - x_s) \delta(y - y_s) \delta(z - z_s) \quad (16)$$

which can easily be verified by performing a Galilean transformation fixing the observer to the fluid in which case the left hand side reduces to equation (14). The boundary conditions remain as before in equation (15).

The equation can now be transformed using the following combination of the Lorentz and Galilean transformations:

$$x \rightarrow X, \quad y \rightarrow Y/\beta, \quad z \rightarrow Z/\beta, \quad t \rightarrow T - MX/(c_0\beta^2) \quad (17)$$

where $\beta^2 = 1 - M^2$. Equation (16) becomes

$$\beta^2 \left[\nabla_0^2 - \frac{1}{\beta^4 c_0^2} \frac{\partial^2}{\partial T^2} \right] \phi_0 = Q(T - k^* M x_s) \delta(x - x_s) \delta(Y/\beta - y_s) \delta(Z/\beta - z_s) \quad (18)$$

where ∇_0 is the gradient operator in the transformed coordinates X, Y, Z and

$$\phi_0(X, Y, Z, T) = \phi(x, y, z, t) \quad k^* = k/\beta^2 \quad (19)$$

For any constant c the following property of generalized functions holds true:

$$\delta(cx) = c^{-1} \delta(x) \quad (20)$$

Applying this equation and assuming a sinusoidal time dependence

$$Q(t) = Q_0 e^{i\omega t} \quad \phi_0(t) = \Phi_0 e^{i\omega t} \quad (21)$$

gives

$$(\nabla_0^2 + k^{*2}) \Phi_0 = Q_1 \delta(X - X_s) \delta(Y - Y_s) \delta(Z - Z_s) \quad (22a)$$

where

$$Q_1 = Q_0 e^{-ik^* M x_s} \quad (22b)$$

Equation (22a) for $M \neq 0$ is identical in form with equation (1) for the $M = 0$ case. The amplitude of the source strength Q_0 which is a constant in equation (1) becomes Q_1 in equation (22a); Q_1 is also a constant in that it does not depend on the independent variables X, Y, Z . Also, the boundary conditions in equation (15) are unchanged by the transformation. Denote the solution for the case $M = 0$ by $\Phi_0(x_s, y_s, z_s; x_o, y_o, z_o, k)$. The solution of equation (16) for the forcing function given by equation (21) is thus found from equation (3) by replacing Q_0 by $Q_0 \exp(-ik^* M x_s)$, k by k^* and x, y, z by X, Y, Z respectively. Finally the result is multiplied by $\exp(i\omega T) = \exp(i\omega t + ik^* M x)$. After inverse transformation from X, Y, Z to x, y, z the result is

$$\phi(x_s, y_s, z_s; x_o, y_o, z_o; k, M, t) = e^{ik^* M (x_o - x_s)} \Phi_0(x_s, \beta y_s, \beta z_s; x_o, \beta y_o, \beta z_o; k) e^{i\omega t} \quad (23)$$

A similar transformation was used by Candel (ref. 7). His transformation and final result can be seen to be essentially the same as the above. For example, his $k_1 = k/\beta$ and $x_1 = x/\beta$; thus, his $\exp(ik_1 M x_1)$ is equivalent to $\exp(ik^* M x)$ above. However, because of the factor k that appears outside the square brackets in equation (3), and because the definition of k^* used here differs from that of Candel, a comparison with Candel's equation (28) might appear to differ from that obtained above. The difference results from the fact that Candel is considering the case of an incident plane wave which is assumed to be the same with and without flow while the present case is concerned with the case of a point source with an output which is affected by the flow.

2. Swept wing

The potential field of a swept wing in a flow satisfies the same equation, equation (16), as for the unswept case. The only difference is in the boundary condition. Equation (15) becomes

$$\partial\phi/\partial y = 0 \quad \text{on } y = 0, \quad x - z \tan \gamma > 0 \quad (24)$$

where γ represents the angle between the leading edge and the z axis; see figure 3. The same transformation given by equation (17) then reduces the problem to the no flow case. The sweep angle γ' in the transformed zero-flow plane is

$$\tan \gamma' = \beta^{-1} \tan \gamma \quad (25)$$

The solution ϕ for the potential field of the source near a swept wing with flow can then be written

$$\phi(x_s, y_s, z_s; x_o, y_o, z_o; k, M, \gamma, t) = \Phi'_0(x_s, \beta y_s, \beta z_s, x_o, \beta y_o, \beta z_o; k', \gamma') e^{i\omega t} \quad (26)$$

where Φ'_0 represents the solution to the no-flow problem in a coordinate system with nonzero γ' ; note the prime on Φ'_0 to distinguish it from Φ which was defined in a coordinate system with Z along the leading edge. Φ does not have γ' as a parameter. The fact that γ' is nonzero means that in order to relate to the previous solution given by equation (3), a coordinate rotation through the angle γ' must be made. The transformed coordinates, denoted by primes, are related to the non-primed coordinates in the zero-flow plane by

$$X' = X \cos \gamma' - Z \sin \gamma' \quad Z' = X \sin \gamma' + Z \cos \gamma' \quad (27)$$

The equation relating the velocity potential for flow to that with no flow and with the z axis along the leading edge is finally

$$\phi(x_s, y_s, z_s; x_o, y_o, z_o; k, M, \gamma, t) = \Phi_0(X'_s, Y'_s, Z'_s; X'_o, Y'_o, Z'_o; k') e^{ik' M(x_o - x) + i\omega t} \quad (28)$$

3. Leading and trailing edge cases

Equation (29) gives a solution to the wave equation which satisfies the boundary condition of no flow through the plate. For the case of a leading edge ($0 < M < 1$) the solution represents the velocity potential, not the pressure. The pressure field for the leading edge case can be found from the momentum relation

$$p = -\rho D\phi/Dt \quad (29)$$

where $D/Dt \equiv \partial/\partial t + U \partial/\partial x$ represents the substantial derivative. The velocity potential for the leading edge case must behave as $x^{1/2}$, in contrast to the pressure and velocity fields which have a $x^{-1/2}$ singularity there. Thus, there is no discontinuity in potential at the leading edge, but there is a discontinuity in pressure. The $x^{1/2}$ behavior of the velocity potential at the leading edge is typical for this type of problem. The same behavior is found, for example, for a two-dimensional plate moving along its normal in an incompressible fluid; this can readily be solved using complex variable mapping techniques.

For the trailing edge case, the behavior is different. Here the imposition of the Kutta condition requires that the pressure field go to zero at the trailing edge. Also, there can be no pressure discontinuity downstream of the trailing edge, although there will, in general, be a discontinuity in the velocity potential. Looking again at the boundary value problem for the leading edge given by Eqs.(15) and (16), the solution is seen to apply to the trailing edge if $M \rightarrow -M$ and if ϕ is taken to represent the pressure field. Thus, with $-1 < M < 0$, equation (28) represents the pressure field of a point pressure monopole in the presence of a trailing edge. With $0 < M < 1$, equation (28) represents the velocity potential of a point velocity-potential-monopole near the leading edge of a semi-infinite zero-thickness flat plate.

Comparing the solutions for the leading and trailing edges, it will be noted that they are solutions for different forcing functions. The leading edge solution is for a monopole in the velocity potential. The trailing edge solution is for a monopole in the pressure field. The monopole in the velocity potential can be interpreted as fluid injected into the

stream through a porous body. The monopole in the pressure field can be interpreted as the same type of source injecting fluid through a porous body but with the addition of a dipole aligned with the flow; another interpretation is that it represents a body in the fluid which pulsates in thickness but which adds no fluid to the flow, in contrast to the first case of fluid added through a porous body.

Because of the difference in source type for leading and trailing edges, it is necessary to normalize the solutions with respect to the incident pressure field, in some manner, before a comparison between the leading and trailing edge solutions can be made.

4. Normalization of the solution

In order to properly gauge the importance of diffraction using the preceding solution, it is necessary to first normalize the solution in some manner. As it stands, equation (3) predicts a diffracted amplitude which is directly proportional to the source strength Q_0 . The most obvious method of normalizing the solutions for leading and trailing edge diffracted pressure is to divide by the pressure that would be present at the observer location in the absence of the half plane. With flow, the solution to the monopole forcing function is

$$\phi_0 = -\frac{Q_0}{4\pi\sigma_{os}} e^{ik^* [M(x_0 - x_s) - \sigma_{os}t] + i\omega t} \quad (30)$$

where

$$\sigma_{os} = \sqrt{(x_0 - x_s)^2 + \beta^2 [(y_0 - y_s)^2 + (z_0 - z_s)^2]}$$

For the trailing edge case ϕ_0 can be taken to be the pressure while for the leading edge case the substantial derivative must be taken. In taking the derivative, only the far-field component will be retained. It is felt that the additional complexity introduced by retaining the near-field terms in the normalizing factors would obscure the meaning of the results. Both the near and far-field terms are present in the actual solution, however, and it is a simple matter to account for the near-field terms in the normalizing factor if desired.

For the trailing edge case the normalizing factor is

$$N_{t.e.} = |\phi_i|_{observer} = \frac{Q_0}{4\pi\sigma_{os}} \quad (31)$$

For the leading edge case

$$N_{l.e.} = \rho_0 \left| \frac{D\phi_i}{Dt} \right|_{observer} = \rho_0 \frac{k Q_0}{4\pi\sigma_{os} \beta^2 c_0} (1 - M \cos \theta_1) \quad (32)$$

with

$$\cos \theta_1 = x_s / \sigma_{os}$$

These factors should be used to normalize the appropriate diffraction relations given previously. The computer program, to be described later, makes this normalization using the exact diffraction solution. (Actually, if kR_1 is large, the asymptotic solution is used, but this loses little in accuracy.)

Before settling on this normalization for the analysis, let us first consider further the properties of the diffraction solution. For present purposes, to simplify matters, let us consider just the asymptotic solution for kR_1 large and for $M = 0$. Then, from Eq.(3) and Eqs.(11) - (13)

$$\phi = Q_0 (ik/8\pi) [I(R) + I(S)] \quad (33)$$

$$\begin{aligned} I(R) &= e^{-ikR} \frac{2i}{kR} \left[1 - e^{-i\pi/4} \frac{R e^{-ik(R_1 - R)}}{2\sqrt{2\pi k r_s r_o R_1} \cos[(\theta_o - \theta_s)/2]} \right] & \tau_R > 0 \\ &\approx e^{-ikR_1 - i\pi/4} \frac{i}{k\sqrt{r_s r_o R_1}} \frac{1}{\sqrt{2\pi k r_s} \cos[(\theta_o - \theta_s)/2]} & \tau_R < 0 \end{aligned} \quad (34)$$

with the restriction that $\theta_o - \theta_s$ not be near π ; i.e., the observer must not be near the edge of the diffraction field. The diffraction component of this result is

$$I_d(R) \approx - \frac{1}{k \sqrt{2\pi k r_s r_o R_1} \cos[(\theta_o - \theta_s)/2]} e^{-ikR_1 + i\pi/4} \quad (35)$$

Combining this with $I_d(S)$ gives

$$\phi_d \approx \frac{Q_o}{(2\pi)^{3/2}} \frac{1}{\sqrt{k r_s r_o R_1}} \frac{\cos(\theta_o/2) \cos(\theta_s/2)}{\cos \theta_o + \cos \theta_s} e^{-ikR_1 - i\pi/4} \quad (36)$$

For $M = 0$, because of the omnidirectionality of the source, it makes no difference whether the normalization is with respect to the pressure at the observer position or at the edge (extrapolated to an equal distance). Also, the solutions for the leading and trailing edges become identical. If equation (36) is normalized using equation (32) with $M = 0$, the result is

$$\frac{\phi_d}{|\phi_{de}|} \approx \sqrt{\frac{2r_s}{\pi k r_o R_1}} \frac{\cos(\theta_o/2) \cos(\theta_s/2)}{\cos \theta_o + \cos \theta_s} e^{-ikR_1 - i\pi/4} \quad (37)$$

This represents the diffraction solution for either the leading or trailing edge case (assuming $M = 0$) normalized by either the pressure at the observer with no plate or the pressure at the edge (extrapolated to equal distance from the source) with no plate. It represents both the normalized potential solution and the normalized pressure since as noted from equation (29) the only difference between the two is the constant factor $-i\omega\rho$ which is present in both the solution and the normalizing factor, and so drops out. Because it is only the diffraction component of the solution, the direct and reflected rays must be added if the observer is not assumed in the shadow zone of the diffraction.

This result is very interesting. Consider the directional behavior of this normalized field. For an observer in the plane $z_o = z_s$, the angular dependence occurs only in the explicit θ_o factor in equation (37). Also, recall that there is no directionality in the normalizing term. The directionality in equation (37) is the same as that for the case of a plane wave incident on an edge. (See, e.g., equation (13) of the paper by Candel (ref. 7), remembering to account for the fact that Candel defines θ and Θ to be the supplements of θ , and θ_s defined here.) If the observer goes to the far field, $r_o \gg r_s$, the amplitude factor (multiplying the directivity) becomes $[2r_s/(\pi k)]^{1/2}/r_o$, and this can readily be shown to be the same for all forcing functions such as dipole, quadrupole, etc.; i.e., take the derivative of the monopole solution and normalize as above with the incident pressure field.

The fact that the same directivity pattern is obtained from two completely different source types (monopole and plane wave) is illustrative of a very powerful result: for the limits of high frequency and far field

$$kR_1 \gg 0 \quad \text{and} \quad r_o \gg r_s \quad (38)$$

the diffraction field for an arbitrary source directivity can be found from that for a monopole source. The two diffraction patterns are equal if normalized by the wave amplitude incident on the edge; that is, the diffraction pattern is dependent only on the ray striking the edge, and not on the general source directivity. The relevant edge point is the one which minimizes the distance from source to edge to observer. Further discussion of this principle can be found in the paper by Keller (ref. 9). It is also described in the report by Boeing (ref. 10).

This is basically a geometric acoustics type of solution in which the incident sound moves along a ray tube to a point on the edge. On reaching the edge, which is assumed thin with respect to the wavelength, the sound diffracts around the edge. Now, the diffraction from any point on the edge is determined by the properties of the incident wave within approximately one wavelength of the point; under the assumption $kr_s \gg 1$, the radius of curvature of the incident wave is much greater than a wavelength and the wavefront can be treated as plane. Thus, the diffracted component of the solution for the limits given by equation (38) is independent of the detailed source directivity, only depending on the amplitude directed at the edge. Once reaching the edge, the ray is diffracted into a conical surface with the z axis being the axis of the cone. For any point on this conical surface, the minimum distance from this point to the source, with the edge as an intermediate point, is along a path from this point to the apex of the cone, and from the apex of the cone to the source. If the observer is in the shadow of the plate, then the only sound reaching the observer is the diffracted sound; if the observer is not in the shadow zone of the plate, then the direct sound (and the reflected sound if the observer is in the shadow zone of the image source) must be added to the diffracted sound. In this case, of course, the source directivity

at these angles, in addition to that of the ray striking the edge, are important.

For nonzero M , the same results apply. The ray paths in the transformed plane correspond with those in the original plane. Since the solutions for a plane wave and a point source agree for $M = 0$, they will agree for $M \neq 0$ since the solution for nonzero M is found by transforming both the plane wave solution and the monopole source solution for $M = 0$ using the same transformation.

Since it is the ray impinging on the edge which determines the diffraction solution, it makes more sense to normalize the solution in terms of the source pressure (in the absence of the plate) at the edge of the plate rather than that at the observer. This will allow the development of a solution for a general source directivity (under the assumptions in equation (38)) to be simply obtained from that for the monopole solution. Since we wish to calculate the sound reduction produced by introducing the plate, it might be thought that this would be given by the solution normalized by the pressure at the observer without the plate. This is true only for the monopole source since this is the source type for which the solution was derived. If a more general solution is desired, the source intensity at the edge must be used for normalization. From this solution normalized by the sound intensity at the edge, the attenuation of the sound from a particular source type produced by introducing a plate can be calculated if the ratio of the directivities at the edge and at the observer are known for this general source type. Also note that if the pressure at the observer is used for the normalization, the normalization pressure would depend on observer location.

In order to make this normalization, first the point at which the ray strikes the edge must be determined. Denoting this point by $(0,0,\zeta)$, the total path length travelled by the ray from source to observer with this edge point as an intermediate point is

$$L = \sqrt{x_s^2 + y_s^2 + (z_s - \zeta)^2} + \sqrt{x_o^2 + y_o^2 + (z_o - \zeta)^2} \quad (39)$$

This distance is minimized by setting the derivative $\partial L / \partial \zeta = 0$ giving

$$\zeta = (r_o z_s + z_o r_s) / (r_o + r_s) \quad (40)$$

For a specific value of ζ there is a linear relation between r_o and z_o . Thus, the locus of observer points related to a specific value of ζ form a cone; that is, a ray will travel from the source to a point ζ on the edge, and from the edge it will diffract into a conical pattern.

This relation is for the zero-flow case without sweep so that for the case with flow and sweep the equation would need to be transformed by Eqs.(18) and (26). Denote this transformed position on the edge by $(x_e, 0, z_e)$. The ray from the source toward this point is

$$\mathbf{h} = -i(x_s - x_e) - j y_s - k(z_s - z_e) \quad (41)$$

where i, j, k are unit vectors along x, y, z . The vector $\mathbf{h}_1 = \mathbf{h} / |\mathbf{h}|$ is normalized to a length r_o to give a vector from the source which grazes the edge and ends in the far field. This normalization is to avoid introducing an r^{-1} effect on the solution due to the difference in distances from the source to the edge and to the observer. With this extrapolation of the vector \mathbf{h} the normalized far-field pressure for a monopole source with $M = 0$ will directly give the attenuation produced by introducing the plate. For more general sources or for $M \neq 0$, the ratio of the directivity in the directions of source and edge must be given to get this result. The pressure at this far-field point, to be used for normalization of the result, is from equation (32) for a leading edge

$$N_{l.e.} = \frac{k Q_o \rho_o}{4\pi c_o \sigma_e} \left[1 + \frac{M(x_s - x_e)}{\sigma_e} \right] \frac{1}{R} \sqrt{(x_s - x_e)^2 + y_s^2 + (z_s - z_e)^2} \quad (42)$$

where

$$\sigma_e = \sigma_{os} |_{x_o = (x_e, 0, z_e)} = \sqrt{(x_s - x_e)^2 + \beta^2 [y_s^2 + (z_s - z_e)^2]} \quad (43)$$

For the trailing edge, from equation (31)

$$N_{t.e.} = \frac{Q_o}{4\pi \sigma_e R} \sqrt{(x_s - x_e)^2 + y_s^2 + (z_s - z_e)^2} \quad (44)$$

In summary, the pressure at an arbitrary field point due to a monopole at an arbitrary source point is obtained from the solution for zero flow using the transformations described above. This is then normalized by the monopole pressure at a distance r_0 from the source along the line touching the edge (assumed to be in the far field). This must then be multiplied by the ratio of pressure along the line touching the edge to that at the observer, but for the particular source being considered.

COMPARISON WITH OTHER SOLUTIONS

Since several of the results presented here have been presented previously by other authors, where possible it is worthwhile to compare results with these previous calculations, if for no other purpose than to verify the computer programs presented here.

The zero Mach number case shown in figure 4 for the directivity of a point source in the vicinity of a half plane can be compared to a similar calculation with the same input parameters in figure 18 of reference 10. The comparison is favorable, with complete agreement to the accuracy that the graph can be read.

The case with flow is slightly more complex. Reference 10 presents figures for leading and trailing edge cases with their parameter $\theta_s = 90^\circ$. Here θ_w is used to denote the angle θ_s used in reference 10. From their figure 17 it appears that θ_w is the wavefront angle, not the angle to the source position; i.e., θ_w is the included angle between c_0 and U . This can be related to the angle θ_s drawn to the source position by recalling that the sound ray will propagate at velocity c_0 along its normal and be convected at velocity U along the flow direction x . Let V denote the propagation speed of a ray (i.e., the vector addition of the fluid velocity and the acoustic velocity) the following equations follow by equating the horizontal and vertical components of ray velocity in terms of V and θ_s to the values expressed in terms of c_0 , U and θ_w :

$$V \sin \theta_s = c_0 \sin \theta_w \quad V \cos \theta_s = c_0 \cos \theta_w - U \quad (45)$$

or

$$\cot \theta_s = \cot \theta_w - M / \sin \theta_w \quad (46)$$

The angle θ_s is the angle from the edge to the source, and for $\theta_w = 90^\circ$, $\cot \theta_s = -M$. Reference 10 gives results for $M = \pm 0.8$; this gives $\theta_s = 141.34^\circ$ for the leading edge case and $\theta_s = 38.66^\circ$ for the trailing edge case.

The results calculated using the present theory for these cases are shown in figures 5a and 5b. The input parameters are matched to those of reference 10: $kr_s = 10$, $z_o = z_s$, the sweep is zero and the observer is in the far field. (Specifically $r_o = 10^3$ is assumed in the computer program.) In each of these plots two curves are shown. The only difference between the two lines is in the normalization; the dashed curve shows the pressure of the monopole source in the presence of the diffracting half-plane normalized by the far-field pressure of the source at the observer with the plane removed. The solid curve shows the same diffracted pressure, but normalized by the extrapolated edge pressure as described previously. The dashed curves are seen to agree well with the corresponding curves given in figure 18 of reference 10, indicating that the results of reference 10 were normalized by the observer pressure with the edge removed.

As was mentioned previously, the ray striking the edge is the one that determines the diffraction field. Since for a general source this ray is independent of the ray toward the observer, it is generally better to normalize the results by the ray striking the edge for an observer in the shadow zone. However, for an observer at a location outside the shadow zone the ray toward the observer will not be intercepted by the plate; for this case normalization by the ray amplitude in the direction of the observer is more meaningful. In fact the curves clearly illustrate that for $\pi - \theta_s < \theta_o < \pi + \theta_s$ where there would be expected to be little effect of the plate (since the observer is outside the shadow zone, but not at a small enough angle that he can see the image source), the curve normalized by the observer pressure is in fact near zero, whereas this is not so clearly evident from the curve normalized by the edge pressure. Perhaps a combination of these normalizations could be made so that when the observer was in the shadow the normalization would be with the edge ray while for an observer in the illuminated region the direct ray would be used.

These curves give the somewhat misleading impression that the edge of the shadow zone gets blown back by the flow. Recall, however, that the source position for the leading and trailing edge cases is different for the data plotted in figures 5. For comparison the results for the case $\theta_w = 90^\circ$ for both leading and trailing edge cases are shown in figures 6. Here it is evident that the edge of the shadow zone remains at $\theta = 270^\circ$, unchanged from the $M = 0$ no flow case. Intuitively one might expect the sound to be blown back toward the plate for the leading edge case. The explanation of this paradox is that the ray propagating toward the edge at the 270° angle must have the normal to its wavefronts canted upstream in order for them to propagate at the 270° angle. After passing the edge, the wavefront angle is not changed; the ray continues propagation along the same line.

BEHAVIOR OF THE SOLUTION

This section will present sample calculations made using the solution presented previously. Before proceeding, however, it is well to determine satisfactory values for the two parameters D and N in the subroutine INTH. D is the dividing point between the exact and the approximate solutions and N determines the number of integration points if the exact solution is used.

A value for D can be found from figure 2. The computer program uses the exact or approximate solution based on the following relations:

$$\begin{aligned} k R_1 \leq D & \quad \text{Exact solution used.} \\ k R_1 > D & \quad \text{Approximate solution used.} \end{aligned} \quad (47)$$

Using Eq.(10) to replace R_1 with t_R , Eqs.(47) become

$$\begin{aligned} kR (\tau_R^2 + 1) \leq D & \quad \text{Exact solution used.} \\ kR (\tau_R^2 + 1) > D & \quad \text{Approximate solution used.} \end{aligned} \quad (48)$$

The first term in these equations is the abscissa in figure 2. With this fact, the figure indicates that at the points $D = 15$ the approximate curve is always very close to the exact curve. This is used as the input to the subroutine INTH.

The value for N can be determined by doing calculations for increasing N values until no further change takes place. With $kR = 10$, going from a value of $N = 5$ to $N = 10$ changed only the fifth digit in the output of the program CINTH, which calls INTH for checking the output. The number of integration steps is scaled with kR so that $N = 10$ should be a good value for the entire range of kR . The behavior of the solution for variations of the input parameters is now considered.

First consider the variation of the solution with Mach number M . First, compare the leading and trailing edge solutions. The only difference in these cases with regard to the computer program is that for the leading edge case $M > 0$ is input while for the trailing edge case $M < 0$ is the appropriate program input. The transformations of x, y, z in equation (17) are the same for leading and trailing edge cases. Thus, the basic solutions for the two cases with the same value of $|M|$ have the same magnitude. This is before normalization and before the derivative in equation (29) is taken for the leading edge case. If the observer is in the far field, only the phase is important in determining the derivative; the same is true for the solution in the absence of the diffracting plane. Also, the variations of the phases for the cases with and without the diffracting plane are the same for the same observer location. Thus, when the solutions for pressure are normalized by the pressures for an observer at the same point without the diffracting plane, the leading and trailing edge cases will give the same results.

This equality of the solutions for the leading and trailing edges, when normalized by the pressure at the same location with no diffracting plane, is evident in figure 7a which is symmetrical about the $M = 0$ axis. The source is at $\theta_s = 90^\circ$ and curves are shown for three different observer angles. For simplicity zero sweep and $z_s = z_o$ are assumed. The particular observer angle $\theta_o = 270^\circ$ gives the same results for normalization by the edge pressure (extrapolated) and observer pressure with no plate since the observer lies on the line from source to edge. Figure 7b shows similar plots except for $\theta_s = 45^\circ$. For both these figures there is little dependence on M for the observer on the line joining source to edge; i.e., on the edge of the shadow zone. For observer positions further back in the shadow zone there appears to be significant dependence on the flow Mach number; generally the effect of M is to increase the shielding for both leading and trailing edge cases.

THE COMPUTER PROGRAMS

Included here are two different main programs and several accompanying subroutines. The main program is DIFRAC. This program computes the diffraction of a single edge, either leading or trailing edge. This main program is used with the subroutines

Main program

Main: DIFRAC	Subroutines:	SDIFF FC	INTH CORD	INTGC SRIS	BESL FRES
--------------	--------------	-------------	--------------	---------------	--------------

Inputs

The inputs to the program are defined in terms of the quantities in figures 1 and 3. They are:

RS = r_s = distance of the source from the z axis.
TS = θ_s = angle of the source from the plane.
AM = M = Mach number; positive for a leading edge and negative for a trailing edge.
GAM = γ = angle of sweep as shown in figure 3.
AK = $k = \omega/c_0 = 2\pi$ frequency/sound speed
RO = r_o = distance of the observer from the z axis.
TO = θ_o = angle of the observer from the plane.
ZO = z_o = z coordinate of the observer.

The inputs can be in any consistent system of units.

Running the program

The program begins by prompting the user to enter a name for the file in which the output will be stored, as well as being written to the screen. The program then prompts the user to input the variables r_s , θ_s , M, γ , k, r_o , θ_o , z_o . The program then outputs these variables as a check, and follows with the output of results for either the leading edge case if $M > 0$ or the trailing edge case if $M < 0$; the pressure, normalized two ways are the first two outputs and the following three give the distance of the source from the edge crossing point of the ray. A sample output is

SOURCE RS = 1.00 THS = 90.0 MACH = .000 GAM = .0 AK = 10.0 RO = 1000.0 THO = 90.0 ZO = .0
2.19322 2.19322 0.0 1.0 .0

SOURCE RS = 1.00 THS = 90.0 MACH = .000 GAM = .0 AK = 10.0 RO = 1000.0 THO = 270.0 ZO = .0
-5.23460 -5.23460 0.0 1.0 .0

SOURCE RS = 1.00 THS = 90.0 MACH = .000 GAM = .0 AK = 10.0 RO = 1000.0 THO = 360.0 ZO = .0
-15.02630 -15.02630 0.0 1.0 .0

Compare these with figure 4; the output values 2.19322, -5.23460 and -15.02630 correspond to dB values for the θ_o angles of 90, 270 and 360 degrees.

Program for intermediate verification of theory

The second main program is CINTH. This is a minor program for checking the subroutine INTH which evaluates the integral I in equation (8). This main program is used with the subroutines

Main: CINTH	Subroutines:	INTH FC	INTGC SRIS	BESL FRES
-------------	--------------	------------	---------------	--------------

CONCLUSIONS

The analytical solution for the diffraction of a plane wave by an infinite span, semi-infinite chord, swept airfoil in a mean flow is a straightforward extension of previous results for diffraction without flow or sweep. The results can readily be computerized to produce a program that can predict the attenuation of a sound wave produced by wing shielding.

REFERENCES

1. Sommerfeld, A.: *Math. Ann.*, **47**, (1896), p.317.
2. Carslaw, H. S.: *Proc. Lond. Math. Soc.*, **30**, (1899), p.121; **18**, (1919), p.291.
3. Macdonald, H. M.: "A Class of Diffraction Problems". *Proc. Lond. Math. Soc.*, **14**, (1915), pp.410-427.
4. Senior, T. B. A.: "The Diffraction of a Dipole Field by a Perfectly Conducting Half-Plane". *Quart. Journ. Mech. and Applied Math.*, **VI**, (1953), pp.101-114.
5. Woods, Betty D.: "The Diffraction of a Dipole Field by a Half-Plane". *Quart. Journ. Mech. and Applied Math.*, **X**, (1957), pp.90-100.
6. Born, Max and Wolf, Emil: *Principles of Optics*. The Macmillan Co., New York, (1964).
7. Candel, S. M.: "Diffraction of a Plane Wave by a Half Plane in a Subsonic and Supersonic Medium". *J. Acoustic Society of America*, **54**, (1973), pp.1008-1016.
8. Erdelyi, A.: *Asymptotic Expansions*. Dover Publications, Inc., New York, (1956).
9. Keller, J. B.: "Geometrical Theory of Diffraction". *J. Acoustic Society of America*, **52**, (1962), pp.116-130.
10. Dunn, D. G., Butzel, L. M., DiBlasi, A., Filler, L., Jacobs, L. D.: Aircraft Configuration Noise Reduction Report, FAA-RD-76-76-I, (1976).
11. Abramowitz, M. A. and Stegun, I. A.: *Handbook of Mathematical Functions*. Dover Publications, Inc., New York, (1968).
12. Boersma, J.: "Computation of Fresnel Integrals". *Math. Comp.*, **14**, (1960), p.380.
13. Sedgewick, Robert: *Algorithms*. Addison-Wesley Publishing Co., Reading, Mass., (1983).

LIST OF SYMBOLS

c_0	Sound speed
E^*, F^*	Combinations of Fresnel integrals defined by equations (12)
$H_1^{(2)}$	Hankel function of the second kind
h	Vector from the source to point e on the edge; defined in equation (41)
h_1	Vector parallel to h with length r_0
I	Integral defined by equation (8)
k	ω/c_0
k^*	Transformed value of k ; defined in equations (19)
M	Flow Mach number
P	Pressure
$Q(t)$	Source strength as a function of time
Q_0	Source strength amplitude; see equations (21)
Q_1	Transformed source strength defined by equations (22)
r_0	Distance of observer from edge
r_s	Distance of source from edge
R	Source-observer distance defined in equations (3)
R_1	Distance defined by equation (6)
S	Image-observer distance defined in equations (3)
v_y	Fluid velocity normal to plate
x, y, z	Cartesian coordinates defined in figure 1
X, Y, Z	Transformed coordinates defined by equations (17)
X', Z'	Transformed and rotated coordinates defined by equations (27)
x_e, z_e	Point on the edge which gives a minimum for the distance between the source and observer.
z_0	z coordinate of observer
z_s	z coordinate of source, taken to be zero for simplicity, losing no generality
β	Prandtl-Glauert factor defined in equations (17)
γ	Sweep angle defined in figure 3
γ'	Sweep angle in transformed plane defined in equation (25)
θ_0	Angle of observer from plane; defined in figure 1
θ_s	Angle of source from plane; defined in figure 1
θ_w	Used to represent the variable θ_0 of Ref. 10
μ_R, μ_s	Integral limits defined in equations (3)
ρ	Fluid density
σ_w	Length parameter defined in equations (30)
σ_e	Value for σ_w for an observer on the edge at point e
τ_R	Parameter defined by equations (9) and (10)
ϕ	Velocity potential including time dependence
ϕ_0	Velocity potential for zero flow including time dependence
ϕ_d	Velocity potential for diffraction component of solution
Φ_0	Velocity potential for zero flow and with time removed
ω	Radian frequency
Subscripts	
o, s	Quantity related to observer or source respectively

Appendix A: Main Program for Calculating Diffraction by an Edge
7/23/84 DIFRAC by R. K. Amiet

```

1      COMPLEX CX, CX1, PHI, PHIP, PHIM, PHI1, PHI1P, PHI1M,
2      1      DPHI, DPHI1, PRLE, PRLE1, AI
3      CHARACTER*12 FNAME
4      AI = CMPLX(0.,1.)
5      WRITE(9,*) ' OUTPUT FILE NAME -'
6      READ(9,*) FNAME
7      OPEN(1,FILE=FNAME,STATUS='NEW')
8      10    WRITE(9,100)
9      100   FORMAT('/ INPUT RS, TS, MACH, GAM, K, RO, TO, ZO, N1=1 END'/)
10     READ (9,*) RS, TS, AM, GAM, AK, RO, TO, ZO, N1
11     IF (N1 .EQ. 1) GO TO 40
12     WRITE(1,300) RS, TS, AM, GAM, AK, RO, TO, ZO
13     300   FORMAT('/ SOURCE',3X,'RS =',F5.2,3X,'THS =',F6.1/' MACH =',
14           1      F5.3,3X,'GAM =',F6.1,3X,'AK =',F7.1,3X,'RO =',F7.1,
15           1      3X,'THO =',F6.1,3X,'ZO =',F7.1)
16     XS = RS*COS(TS/57.2958)
17     YS = RS*SIN(TS/57.2958)
18     ZS = 0.
19     B2 = 1.- AM*AM
20     B = SQRT(B2)
21     AKX = AK/B2
22     XO = RO*COS(TO/57.2958)
23     YO = RO*SIN(TO/57.2958)
24     CALL CORD(XS,YS,ZS,XO-.01,YO,ZO,GAM,B,RSX,TSX,ROX,TOX,ZOX,XE,ZE)
25     CALL DIFF1(RSX,TSX,ROX,TOX,ZOX,AKX,PHIM,PHI1M,15.,10)
26     CALL CORD(XS,YS,ZS,XO+.01,YO,ZO,GAM,B,RSX,TSX,ROX,TOX,ZOX,XE,ZE)
27     CALL DIFF1(RSX,TSX,ROX,TOX,ZOX,AKX,PHIP,PHI1P,15.,10)
28     CALL CORD(XS,YS,ZS,XO,YO,ZO,GAM,B,RSX,TSX,ROX,TOX,ZOX,XE,ZE)
29     CALL DIFF1(RSX,TSX,ROX,TOX,ZOX,AKX,PHI,PHI1,15.,10)
30     CX = CEXP(AI*AKX*AM*(XO - XS))
31     CX1 = CEXP(AI*AKX*AM*.01)
32     PHI = PHI*CX
33     PHI1 = PHI1*CX
34     DPHI = 50.*CX*(PHIP*CX1 - PHIM/CX1)
35     DPHI1 = 50.*CX*(PHI1P*CX1 - PHI1M/CX1)
36     PRLE = -(AK*PHI + AM*DPHI)
37     PRLE1 = -(AK*PHI1 + AM*DPHI1)
38     PPTE = 20.*ALOG10(CABS(PHI/PHI1))
39     PPLE = 20.*ALOG10(CABS(PRLE/PRLE1))
40     XOS = XO - XS
41     YOS = YO - YS
42     ZOS = ZO - ZS
43     SGOS = SQRT(XOS*XOS + B2*(YOS*YOS + ZOS*ZOS))
44     ROS = SQRT(XOS*XOS + YOS*YOS + ZOS*ZOS)
45     XSE = XS - XE
46     ZSE = ZS - ZE
47     SGSE = SQRT(XSE*XSE + B2*(YS*YS + ZSE*ZSE))
48     RSE = SQRT(XSE*XSE + YS*YS + ZSE*ZSE)
49     CORTE = SGOS*RSE/(SGSE*ROS)
50     CORLE = CORTE*(1.+ AM*XSE/SGSE)/(1.- AM*XOS/SGOS)
51     PNORLE = PPLE - 20.*ALOG10(CORLE)
52     PNORTE = PPTE - 20.*ALOG10(CORTE)
53     PP = PPLE
54     PNOR = PNORLE

```

```

55      IF (AM .LT. 0.) PP = PPTE
56      IF (AM .LT. 0.) PNOR = PNORTE
57      WRITE(9,600) PP, PNOR, XSE, YS, ZSE
58      WRITE(1,600) PP, PNOR, XSE, YS, ZSE
59 600   FORMAT(1X,2F12.5,3F6.1)
60      GO TO 10
61 40    CLOSE(1)
62      END

```

COMMENTS: This is the main executive routine for calling the various diffraction subroutines, and for normalizing the resulting output by the appropriate pressure.

```

3-7      Open file for output.
8-15     Prompt for inputs.
        RS = Distance of source from z axis.
        TS = Angle of source from plane.
        MACH = Flow Mach no.;  $M > 0 \Rightarrow$  leading edge;  $M < 0 \Rightarrow$  trailing edge.
        GAM = Sweep angle of airfoil;  $GAM = 0 \Rightarrow z$  along leading edge.
         $AK = \omega/c_0$ 
        RO = Distance of observer from z axis.
        THO = Angle of source from plane.
        ZO = Distance between  $z = 0$  plane & plane containing observer and normal to z axis.
16-18    XS, YS, ZS = the x, y, z distances of the source from origin; the origin is located so that the x axis is
        along the flow vector, the y axis is normal to the plane containing the airfoil, and the origin is on the
        leading edge.
        ZS is taken to be zero; this fixes the origin.
19-20    B = Prandtl-Glauert factor.
21       AKX = wavenumber in transformed plane.
22-23    XO & YO = the x and y distances of the observer from the origin.
24-29    First the transformed coordinates (with an X ending) are found; these are then used in the subroutine
        SDIFF1 for the no-flow solution. The 0.01 deviations from XO are used to find the axial derivative.
30-31    Phase factor relating the no-flow solution to the flow solution. CX1 is the additional factor for solutions
        with 0.01 difference in XO.
32-33    Relating the flow and the non-flow pressures for the TE case.
34-35    The x derivatives needed for the calculation of pressure from potential using equation (28).
36-37    Pressure calculation for the leading edge case. PHI is the pressure for the trailing edge case and PRLE is the
        pressure for the leading edge case. The 1 ending on these two variables denotes the pressure for the case
        with no plate.
38-39    DB calculations for leading and trailing edge cases after normalizing by the pressure in the absence of the
        plate.
40-42    Distances between source and observer.
43        $\sigma$  at observer with source at origin.
44       Source-observer distance.
45-46    x and z distances of source from edge-crossing point.
47        $\sigma$  at edge-crossing point with source as origin.
48       Distance between edge-crossing point and source.
49-50    Ratio of pressures at observer and edge-crossing point; line 49  $\Rightarrow$  trailing edge case;
        line 50  $\Rightarrow$  leading edge case.
51-52    DB levels for pressures normalized by that at edge, extrapolated.
53-56    Print either LE case or TE case, not both.

```

Appendix B: Subroutine for Calculation of Integral in Equation (8)

8/12/84 INTH by R. K. Amiet

```

1      SUBROUTINE INTH(UR,RK,D,N,P,J)
2      COMPLEX P, AI, E, FTR1
3      AI = CMPLX(0.,1.)
4      RRK = RK*COSH(UR)
5      IF (RRK .GT. D) GO TO 10
6      M = N*RRK + 1
7      CALL INTGC(0.,UR,RK,M,P)
8      P = .5*(CEXP(-AI*RK)/RK - AI*P)
9      J = 0
10     GO TO 20
11 10   SQ1 = SQRT((RK + RRK)*RRK)
12     TR = RRK - RK
13     CALL FRES(TR,E)
14     FTR1 = CMPLX(.5,-.5) - CONJG(E)
15     P = FTR1*CEXP(AI*(.7853982 - RK))/SQ1
16     IF (UR .GT. 0.) P = CEXP(-AI*RK)/RK - P
17     J = 1
18 20   RETURN
19     END

```

Comments: This subroutine calculates the integral in the equation following equation (3.2) in the paper by Betty Woods. This is the same as the integral I in equation (8) here multiplied by $(-i/2)$.

```

1      The inputs to the subroutine are UR, RK, D and N. UR =  $\mu_R$  in equation (2), RK =  $R \cdot k$  with R given by
      equation (3) and k by equation (1). D defines the cutoff point for switching from the exact to the
      asymptotic solution; for  $k \cdot R_1 > D$ , the asymptotic solution is used. The parameter N specifies the number
      of integration points for exact solution;  $N = 10$  appears to be sufficiently large.
4      RRK =  $k \cdot R_1$  as can be seen from equation (6).
5      Check whether to use exact or asymptotic solution. Go to 10 for the asymptotic solution.
6      M will be proportional to the number of integration points. M increases as  $N \cdot k \cdot R \cdot \cosh \mu_R$  since this is
      proportional to the range of the argument of  $H_1^{(2)}$  in equation (8).
7      The integration subroutine INTGC is called for the integration needed in equation (8). The inputs are the
      integration limits 0 and  $\mu_R$ , the parameter  $R \cdot k$  and the number M which is proportional to the number of
      integration steps.
8      Integrated result with limits  $\pm \infty$  from equation (4) is added to result with limits  $-\mu_R, 0$  in equation (8).
9      J is a program output showing whether the exact or the approximate solution was used.
      J = 0  $\Rightarrow$  exact solution; J = 1  $\Rightarrow$  approximate solution.
10     Skip over the approximate solution.
11     SQ1 is the radical  $[R_1(R_1 + R)]^{1/2}$  in equation (11).
12-13  Since the subroutine FRES calculates  $C_2$  and  $S_2$ , and since equation (11) is defined in terms of C and S, the
      input to FRES must be the argument in equation (11) squared and multiplied by  $\pi/2$ ; see Ref. 11 p. 300.
      TR used here is  $\tau_R(R \cdot k)^{1/2}$ .
14     FTR1 is  $F^*$  in equation (11).
15     The remaining factors in equation (11) multiply  $F^*$ , and the result is multiplied by  $(-i/2)$ .
16     For  $\mu_R > 0$  the final result is composed of an integral from 0 to  $\infty$  and one from  $-\tau_R$  to 0.
17     Same comment as 9.

```

Appendix C: Subroutine for Calculation of R, S, μ_R and μ_S 8/3/84 SDIFF by R. K. Amiet

```

1      SUBROUTINE DIFF1 (RS, THS, RO, THO, ZO, AK, P, P1, D, N)
2      COMPLEX P1, PR, PS, P, AI, AX
3      AI = CMPLX(0., 1.)
4      C1 = COS(.5*(THS - THO))
5      C2 = COS(.5*(THS + THO))
6      S1 = SIN(.5*(THS - THO))
7      S2 = SIN(.5*(THS + THO))
8      RMR = (RS - RO)**2 + ZO**2
9      R1K = SQRT(RMR + 4.*S1**2*RS*RO)*AK
10     S1K = SQRT(RMR + 4.*S2**2*RS*RO)*AK
11     SQ1 = 2.*SQRT(RS*RO)*AK
12     IF (R1K .LT. 1.E-5) THEN
13         ARG1 = SQ1*C1*1.E5
14     ELSE
15         ARG1 = SQ1*C1/R1K
16     END IF
17     IF (S1K .LT. 1.E-5) THEN
18         ARG2 = SQ1*C2*1.E5
19     ELSE
20         ARG2 = SQ1*C2/S1K
21     END IF
22     UR = ALOG(ABS(ARG1) + SQRT(ARG1**2 + 1.))*SIGN(1., ARG1)
23     US = ALOG(ABS(ARG2) + SQRT(ARG2**2 + 1.))*SIGN(1., ARG2)
24     CALL INTH(UR, R1K, D, N, PR, J1)
25     CALL INTH(US, S1K, D, N, PS, J2)
26     AX = -AI*R1K
27     P1 = CEXP(AX)/R1K
28     P = PR + PS
29     RETURN
30     END

```

Comments: This subroutine calculates R, S, μ_R and μ_S as defined in equation (3) from the input values of the source and observer coordinates. These parameters are then used in the subroutine INTH to calculate the two integrals in equation (3) multiplied by $(-i/2)$. These two integrals are then added to give the final result.

4-7 Sine and cosine of the angles used in equation (3).
8-10 Calculation of $k \cdot R$ and $k \cdot S$ where R and S are defined in equation (3).
11 Calculation of factor in μ_R and μ_S in equation (3).
12-16 Calculation of the argument in the square brackets in equation (3) in the definition of μ_R . If the denominator in line 15 is very small (which will be true if the observer is very near the source) then a very large value is used for the argument to avoid division by zero.
17-21 Same as 12-16 except for μ_S rather than μ_R . The argument in line 20 will be small if the observer is near the image source.
22-23 $UR = \mu_R$ and $US = \mu_S$.
24-25 Calculation of the integrals in equation (3) times factor $(-i/2)$.
26-27 Calculation of free-field source pressure times factor $4\pi/(Q_0 k)$. See line 28 comment.
28 Source pressure with halfplane present times factor $4\pi/(Q_0 k)$.

Appendix D: Subroutine for Transforming Sweep and Flow **8/3/84 CORD by R. K. Amiet**

```

1      SUBROUTINE CORD(XS,YS,ZS,XO,YO,ZO,G,B,RSX,TSX,ROX,TOX,ZOX,XE,ZE)
2      CA = COS(G/57.2958)
3      SA = SIN(G/57.2958)
4      SQ = SQRT(SA*SA + B*B*CA*CA)
5      CX = B*CA/SQ
6      SX = SA/SQ
7      XOX = XO*CX - B*ZO*SX
8      YOX = YO*B
9      ZOX = XO*SX + B*ZO*CX
10     XSX = XS*CX - B*ZS*SX
11     YSX = YS*B
12     ZSX = XS*SX + B*ZS*CX
13     RSX = SQRT(XSX*XSX + YSX*YSX)
14     ROX = SQRT(XOX*XOX + YOX*YOX)
15     TSX = ATAN2(YSX,XSX)
16     TOX = ATAN2(YOX,XOX)
17     IF (TSX .LT. 0) TSX = TSX + 6.28318531
18     IF (TOX .LT. 0) TOX = TOX + 6.28318531
19     ZET = ZOX - (ZOX - ZSX)*ROX/(ROX + RSX)
20     XE = ZET*SX
21     ZE = ZET*CX/B
22     ZOX = ZOX - ZSX
23     RETURN
24     END

```

Comments: This subroutine takes the coordinates for a non zero flow situation with airfoil sweep and transforms to a coordinate system with zero flow and zero sweep. It also calculates the coordinates of the edge point at which the ray strikes, in real coordinates.

2-3 Sine and cosine of the sweep angle G or γ .
4-6 Sine and cosine of the transformed angle γ' defined by equation (25).
7-12 Coordinates x,y,z transformed first to X,Y,Z system as in equations (17), then rotated through angle γ' as in equations (27).
13-16 Transformed coordinates put in terms of polar coordinates r and θ .
17-18 Angles to source and observer must be $0 < \theta < 2\pi$. Negative angles not permitted because of the barrier.
19 The value of ζ , the edge crossing point in equation (40), is calculated in a coordinate system with zero flow and the z axis along the airfoil leading edge.
20-21 The coordinates of ζ in the real system are calculated.
22 The program INTH for no flow assumes that the z coordinate of the source is zero.

Appendix E: Subroutine for Simpson's Rule Integration

8/12/84 INTGC by R. K. Amiet

```

1      SUBROUTINE INTGC (A, B, C, N, SUM)
2      COMPLEX D, SUM
3      AN = N
4      DEL = .5 * (B-A) / AN
5      N2 = 2 * N - 1
6      X = A
7      M = 2
8      MB = 2
9      CALL FC (A, C, SUM)
10     CALL FC (B, C, D)
11     SUM = SUM + D
12     DO 50 I=1, N2
13         X = X + DEL
14         M = -M
15         MB = MB - M
16         BM = MB
17         CALL FC (X, C, D)
18         SUM = SUM + BM * D
19 50    CONTINUE
20     SUM = SUM * DEL / 3.
21     RETURN
22     END

```

Comments: This subroutine performs a simple Simpson's rule integration.

```

1      Inputs are
      A = lower integral limit
      B = upper integral limit
      C = constant used in integrand
      N = # of integration points
4      DEL = 1/2 of step size.
9-10   Find the value of the integrand FC at the two limits A and B.
12-19  Evaluation of integrand at intermediate points.
20     Multiplication by step size divided by 6.

```

Appendix F: Subroutine for Evaluation of Fresnel Integrals
8/12/84 FRES by R. K. Amiet

```

1      SUBROUTINE FRES(X,E)
2      DIMENSION A(12), B(12), C(12), D(12)
3      COMPLEX AI, E
4      AI = CMPLX(0.,1.)
5      IF (X .GT. 4) GO TO 10
6      Y = X/4.
7      A(1) = 1.59576914
8      A(2) = -1.702E-6
9      A(3) = -6.808568854
10     A(4) = -.000576361
11     A(5) = 6.920691902
12     A(6) = -.016898657
13     A(7) = -3.05048566
14     A(8) = -.075752419
15     A(9) = .850663781
16     A(10) = -.025639041
17     A(11) = -.15023096
18     A(12) = .034404779
19     B(1) = -3.3E-8
20     B(2) = 4.255387524
21     B(3) = -9.281E-5
22     B(4) = -7.7800204
23     B(5) = -.009520895
24     B(6) = 5.075161298
25     B(7) = -.138341947
26     B(8) = -1.363729124
27     B(9) = -.403349276
28     B(10) = .702222016
29     B(11) = -.216195929
30     B(12) = .019547031
31     CALL SRIS(A,Y,12,SA)
32     CALL SRIS(B,Y,12,SB)
33     E = EXP(AI*X)*SQRT(Y)*(SA - AI*SB)
34     GO TO 20
35 10   Y = 4./X
36     C(1) = 0.
37     C(2) = -.024933975
38     C(3) = 3.936E-6
39     C(4) = .005770956
40     C(5) = .000689892
41     C(6) = -.009497136
42     C(7) = .011948809
43     C(8) = -.006748873
44     C(9) = .00024642
45     C(10) = .002102967
46     C(11) = -.00121793
47     C(12) = .000233939
48     D(1) = .19947114
49     D(2) = 2.3E-8
50     D(3) = -.009351341
51     D(4) = 2.3006E-5
52     D(5) = .004851466
53     D(6) = .001903218
54     D(7) = -.017122914

```

```

55      D(8) = .029064067
56      D(9) = -.027928955
57      D(10) = .016497308
58      D(11) = -.005598515
59      D(12) = .000838386
60      CALL SRIS(C,Y,12,SC)
61      CALL SRIS(D,Y,12,SD)
62      E = .5*(1 + AI) + EXP(AI*X)*SQRT(Y)*(SC - AI*SD)
63      20  RETURN
64      END

```

Comments: This subroutine is for calculation of the Fresnel integrals. It is based on reference 12.

```

5      The calculation is divided into small and large x approximations. The small x ( $x < 4$ ) approximation is
      given in lines 6-34. The large x ( $x > 4$ ) approximation is given in lines 35-62.
7-30   Input constants for the small x polynomial approximation.
31-32  Evaluations of the polynomials for the small x approximation.
33     Final evaluation of the Fresnel integrals  $C_2(x) + iS_2(x)$  for an input x.
36-59  Input constants for the large x polynomial approximation.
60-61  Evaluations of the polynomials for the large x approximation.
62     Final evaluation of the Fresnel integrals  $C_2(x)$  and  $S_2(x)$  for an input x.

```

Appendix G: Subroutine for Calculation of Integrand in Equation (8)

8/12/84 FC by R. K. Amiet

```

1      SUBROUTINE FC(X,C,F)
2      COMPLEX F, AI
3      AI = CMPLX(0.,1.)
4      Y = C*COSH(X)
5      CALL BSL(Y,AJ0,AJ1,Y0,Y1)
6      F = AJ1 - AI*Y1
7      RETURN
8      END

```

Comments: This subroutine calculates the value of the integrand in equation (8).
The inputs are X corresponding to μ in equation (8) and C corresponding to kR .

```

4      Argument of the Hankel function.
6      F is the Hankel function of the second kind.

```

Appendix H: Subroutine for Calculation of the Bessel Functions 1976 BESL by R. K. Amiet

```

1      SUBROUTINE BSL(X, J0, J1, Y0, Y1)
2      REAL J0, J1
3      PI = 3.1415927
4      Y = X/3.
5      IF (Y-1.) 10, 10, 20
6 10    Z2 = Y**2
7      Z4 = Z2**2
8      Z6 = Z4*Z2
9      Z8 = Z4**2
10     Z10 = Z8*Z2
11     Z12 = Z6**2
12     J0 = 1.- 2.2499997*Z2 + 1.2656208*Z4 - .3163866*Z6
13         + .0444479*Z8 - .0039444*Z10 + .00021*Z12
14     Y0 = 2.*J0*ALOG(X/2.)/PI + .36746691 + .60559366*Z2
15         - .74350384*Z4 + .25300117*Z6 - .04261214*Z8
16         + .00427916*Z10 - .00024846*Z12
17     J1 = (.5 - .56249985*Z2 + .21093573*Z4 - .03954289*Z6
18         + .00443319*Z8 - .00031761*Z10 + .00001109*Z12)*X
19     Y1 = 2.*J1*ALOG(X/2.)/PI + (-.6366198 + .2212091*Z2
20         + 2.1682709*Z4 - 1.3164827*Z6 + .3123951*Z8
21         - .0400976*Z10 + .0027873*Z12)/X
22     GO TO 30
23 20    Z2 = Y**2
24     Z3 = Z2*Y
25     Z4 = Z2**2
26     Z5 = Z4*Y
27     Z6 = Z3**2
28     F0 = .79788456 -.00000077/Y -.00552740/Z2 -.00009512/Z3
29         + .00137237/Z4 - .00072805/Z5 + .00014476/Z6
30     T0 = X-.78539816 -.04166397/Y-.00003954/Z2 +.00262573/Z3
31         - .00054125/Z4 - .00029333/Z5 + .00013558/Z6
32     S = SQRT(X)
33     J0 = F0*COS(T0)/S
34     Y0 = F0*SIN(T0)/S
35     F1 = .79788456 +.00000156/Y +.01659667/Z2 +.00017105/Z3
36         - .00249511/Z4 + .00113653/Z5 - .00020033/Z6
37     T1 = X -2.3561945 +.12499612/Y +.0000565/Z2-.00637879/Z3
38         + .00074348/Z4 + .00079824/Z5 - .00029166/Z6
39     J1 = F1*COS(T1)/S
40     Y1 = F1*SIN(T1)/S
41 30    RETURN
42     END

```

Comments: This subroutine calculates the Bessel functions J_0 , J_1 , Y_0 , Y_1 .

5 Two x ranges: $x < 3$ and $x > 3$. Small x range: lines 6-22, and the high x range: lines 23-40.
12-15 Equations (9.4.1) and (9.4.2) of reference 11, pp. 369.
16-20 Equations (9.4.4) and (9.4.5) of reference 11, pp. 370.
28-34 Equation (9.4.3) of reference 11, pp. 369. Polynomial approximations.
35-40 Equation (9.4.6) of reference 11, pp. 370.

Appendix I: Program for Calling the Subroutine INTH 7/21/84 CINTH by R. K. Amiet

```

1      COMPLEX P
2      CHARACTER*10 FNAME
3      WRITE(9,*) ' OUTPUT FILE NAME - '
4      READ(9,*) FNAME
5      OPEN(1,FILE=FNAME,STATUS='NEW')
6      10  WRITE(9,100)
7      100 FORMAT(/1X,'INPUT RK, D, N, J (CLOSE FOR J>0)'/)
8      READ(9,*) RK, D, N, J
9      IF (J .GT. 0) GO TO 20
10     WRITE(9,300) RK, D, N
11     WRITE(1,300) RK, D, N
12     300 FORMAT(/1X,2F7.2,I4)
13     DO 50 I=1,50
14         SQT = SQRT(RK)
15         TR = - .1*I/SQT
16         G = TR/SQRT(2.)
17         UR = 2.*ALOG(G + SQRT(G*G + 1.))
18         CALL INTH(UR,RK,D,N,P,J)
19         APRK2 = RK*SQRT(2.*(TR*TR+1)*(TR*TR+2))*CABS(P)
20         TRRK = TR*SQT
21         WRITE(9,400) TR, TRRK, APRK2, J
22         WRITE(1,400) TR, TRRK, APRK2, J
23     400 FORMAT(1X,3E13.5,I4)
24     50  CONTINUE
25     GO TO 10
26     20  CLOSE(1)
27     END

```

Comments: The program steps through TR corresponding to τ_R in equation (10b). The step size is adjusted in line 15 according to the size of RK in order to collapse the approximate calculations into a single curve independent of the size of RK. This is done by making the step size in the argument of the Fresnel integral in equation (11) independent of RK. The results should be plotted against TRRK calculated in line 20; TRRK is proportional to the step number as desired while TR is not. In line 19 all the factors except CABS(P) are for normalizing the output to be independent of $k \cdot R$ for the asymptotic solution.

- 2-5 For inputting filename.
- 6-9 Prompts for inputs of $R \cdot k$, D, N and J; inputting $J > 0$, closes the output file and ends the session.
- 10-12 Writes the above inputs to the screen and to the output file for verification.
- 13-24 Loop to step through τ_R , the integral limit.
- 14-15 τ_R is normalized so that the step size of the argument of F^* is the same for all values of Rk .
- 16-17 μ_R is calculated from τ_R using equation (9).
- 18 The integral I in equation (8) is calculated and multiplied by $(-i/2)$. This is the integral in the equation following equation (3.2) of reference 5.
- 19 CABS(P) is the absolute value of the integral in line 18. All the remaining factors are for cancelling factors other than F^* in equation (11). The factor RK appears explicitly as $R \cdot k$ in equation (11). The two factors with $TR \cdot TR$ come from substituting for R_1/R using equation (10). This can also be seen by backtracking a step to equation (8). For the approximation, τ_R is substituted for τ in the radical in the denominator. The result must be multiplied by a factor of 1/2 since the program is calculating the text integral I_1 multiplied by a factor $(-i/2)$. Finally, the factor $2^{1/2}$ comes from the limit of $F^*(x) \rightarrow 2^{-1/2}$ as $x \rightarrow 0$.
- 20 TRRK is proportional to the step number, independent of the value of $R \cdot k$, whereas TR will not be. Since the argument of F^* in equation (11) is proportional only to the step number, the result is plotted against TRRK so that the plot will be independent of Rk .
- 21-23 The results are output to the screen and to the output file.
- 25 Go back to prompt for new inputs.

Appendix J: Subroutine for Calculating a Power Series

8/12/84 SRIS by R. K. Amiet

```
1      SUBROUTINE SRIS (A, X, N, SUM)
2      DIMENSION A(15)
3      SUM = A(N)
4      DO 50 I=1, N-1
5          J = N - I
6          SUM = SUM*X + A(J)
7      50 CONTINUE
8      RETURN
9      END
```

Comments: This subroutine calculates a power series in the variable x given the array of constants A , the variable x and the number of terms N . The program uses Horner's rule; see e.g., reference 13.

3 This term will be multiplied by x a total of $N - 1$ times.
4-7 The $A(J)$ term will be multiplied by x a total number of $J - 1$ times.

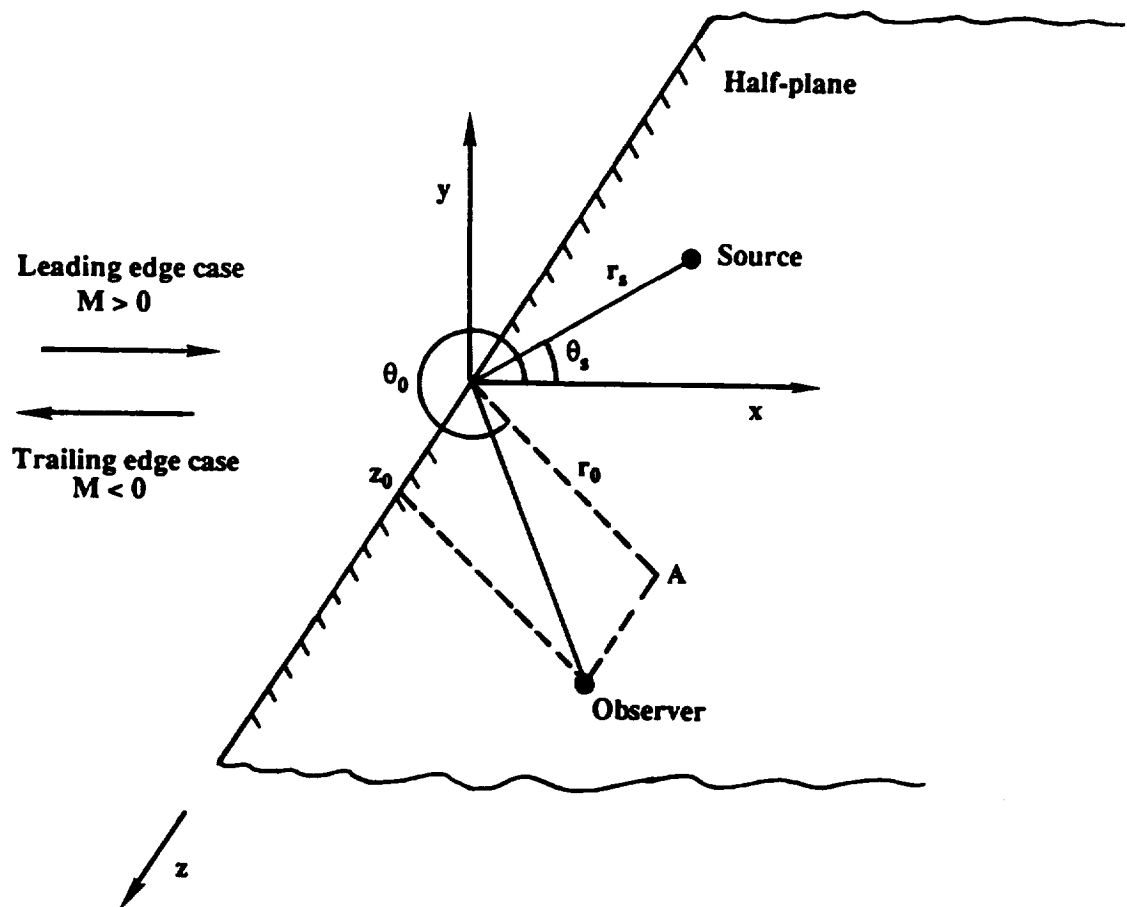


Figure 1: Geometry of the diffraction problem. The half plane lies in the $y = 0$ plane. Point A is the projection of the observer location on the x,y plane. The source lies in the x,y plane. The zero sweep case is shown.

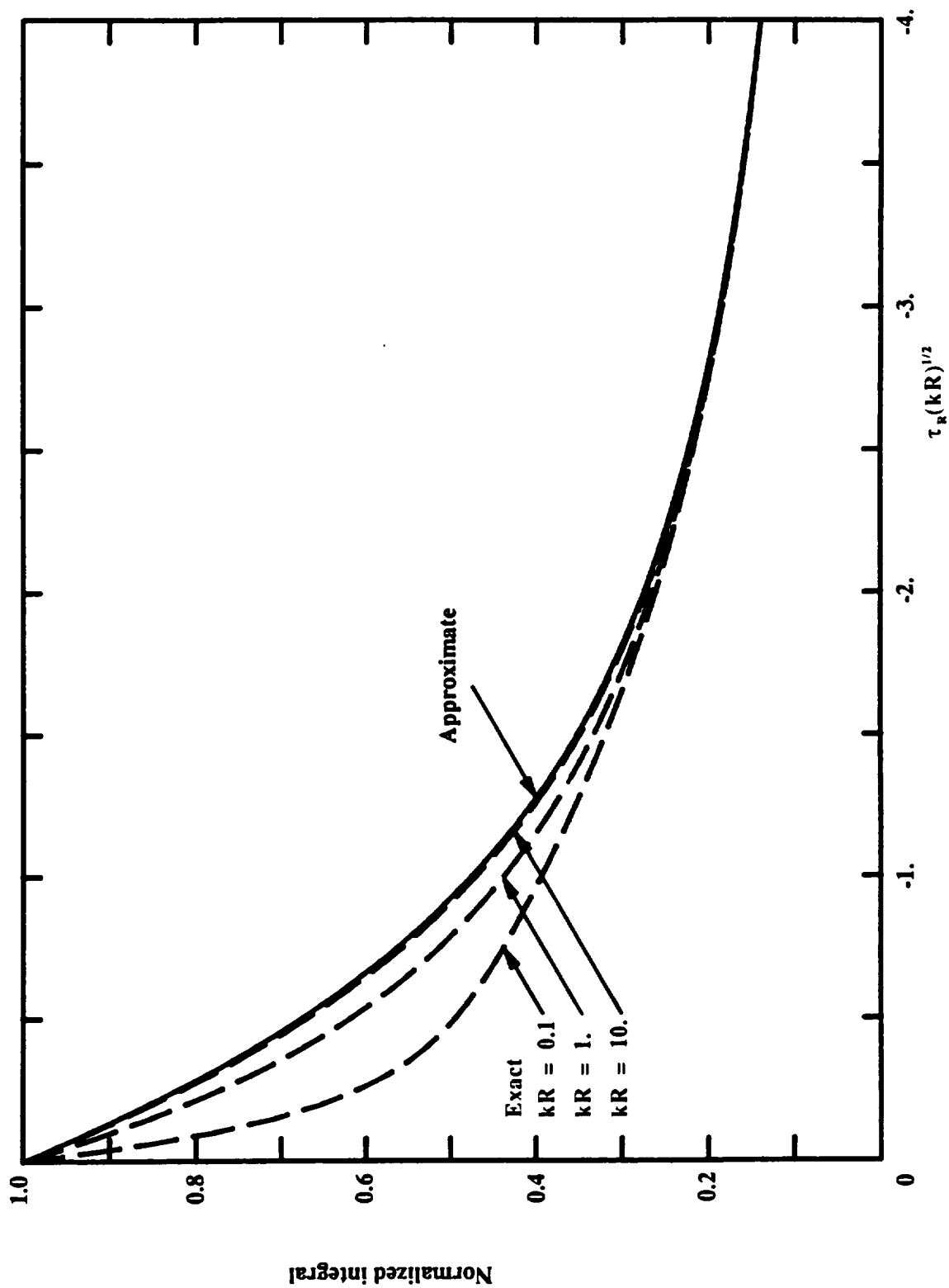


Figure 2: Variation of the integral I with kR . See equation (11) and the paragraph preceding section B for a description of the normalization of I. The exact curves use $D = 100$ and $N = 8$.

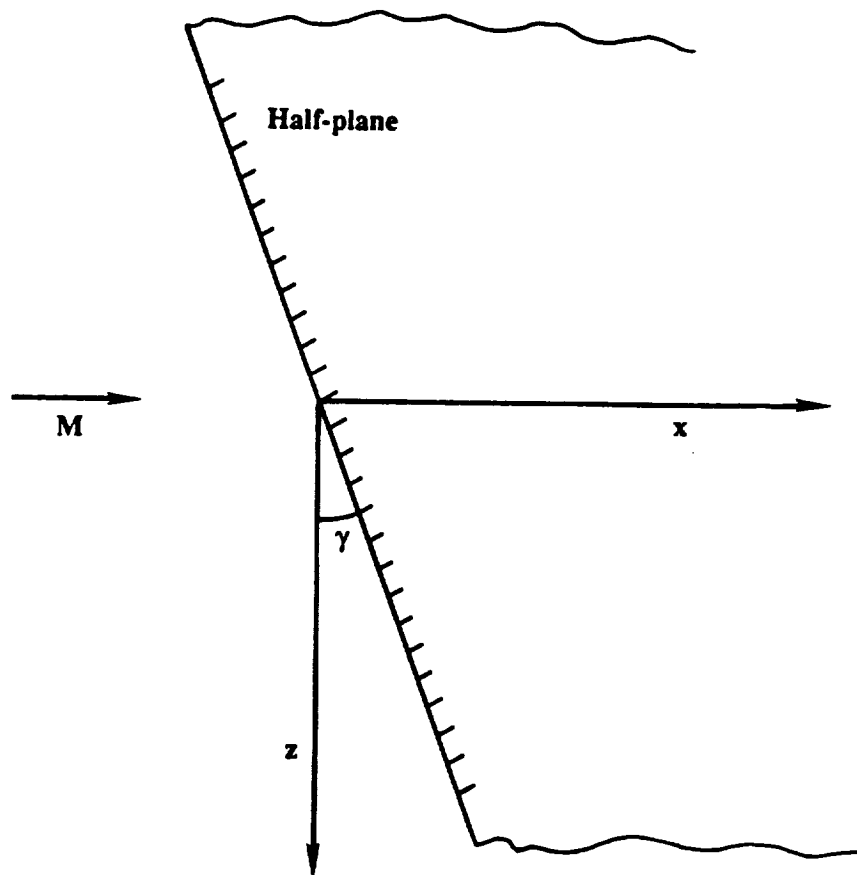


Figure 3: Definition of the sweep angle γ .

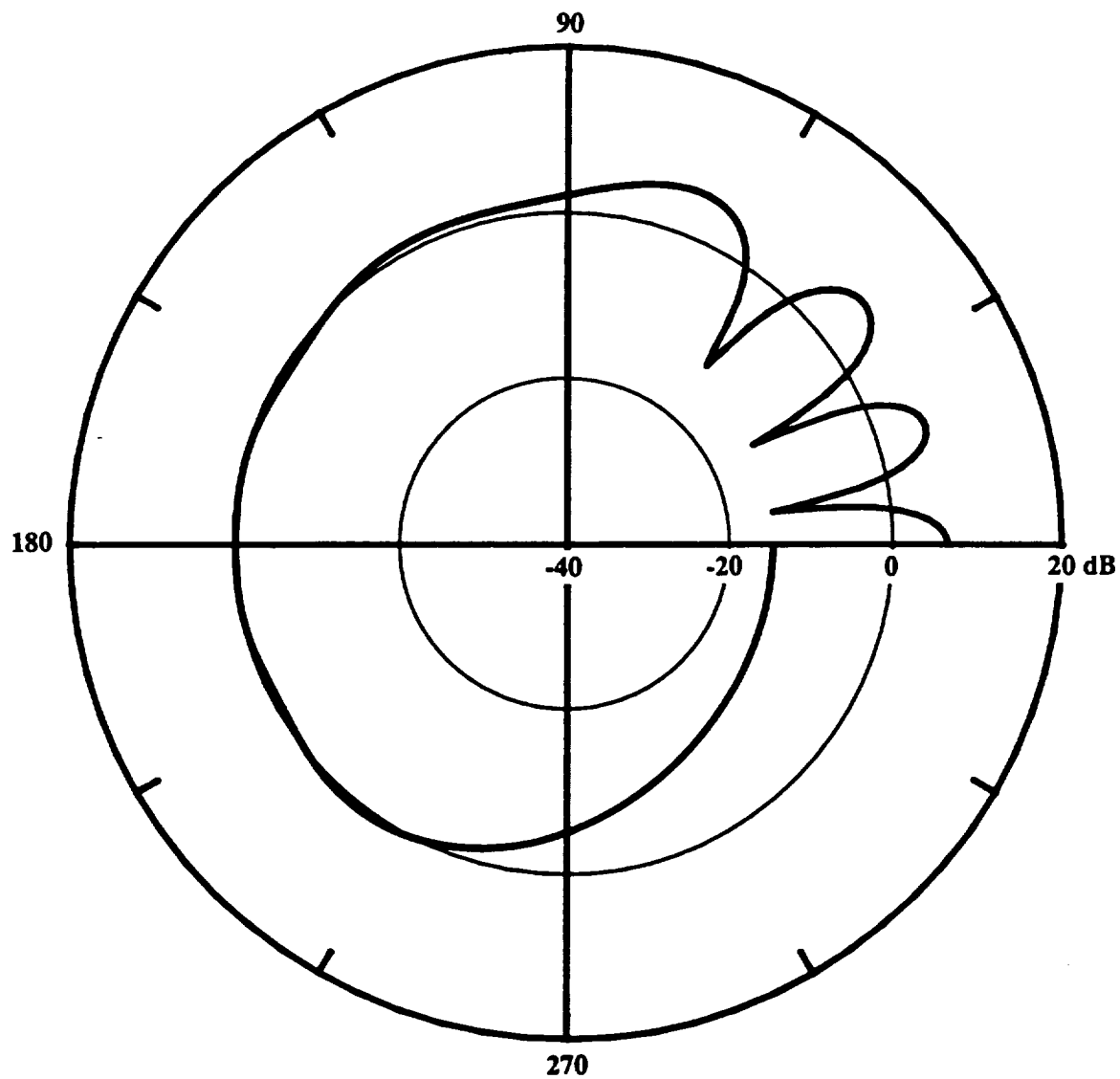


Figure 4: Normalized directivity of a point source diffracted by an edge for the zero flow case.
 $r_s = 1$, $r_o = 1000$, $k_o = 10$, $\theta_s = 90$, $M = 0$, $\gamma = z_o = 0$.

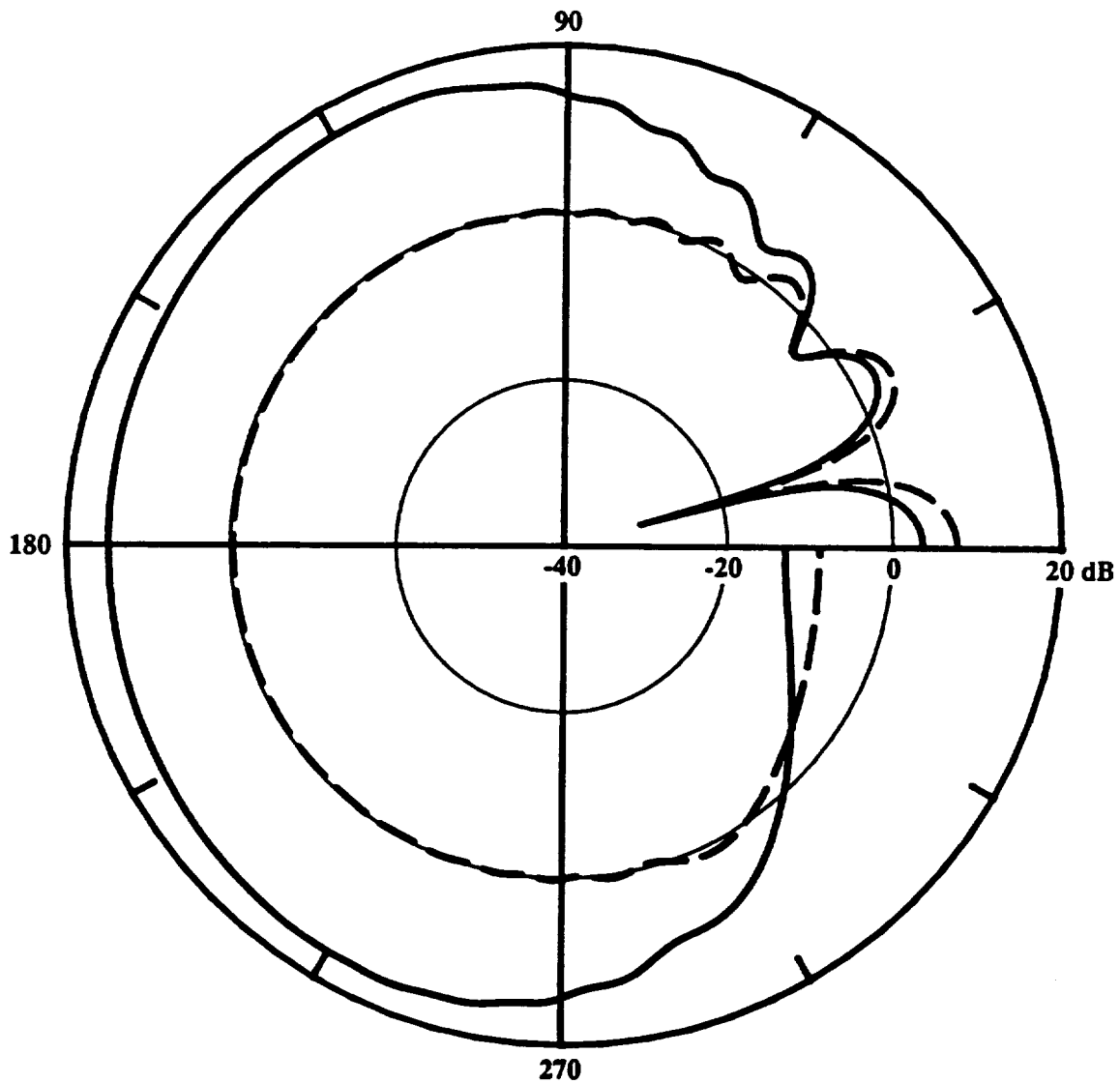


Figure 5a: Normalized directivity of a point source diffracted by a leading edge in a flow; observer directly above the retarded position of the edge; i.e., $\theta_o = 90$.

$r_i = 1$, $r_o = 1000$, $k_o = 10$, $\theta_i = 141.34$, $M = 0.8$, $\gamma = z_o = 0$.

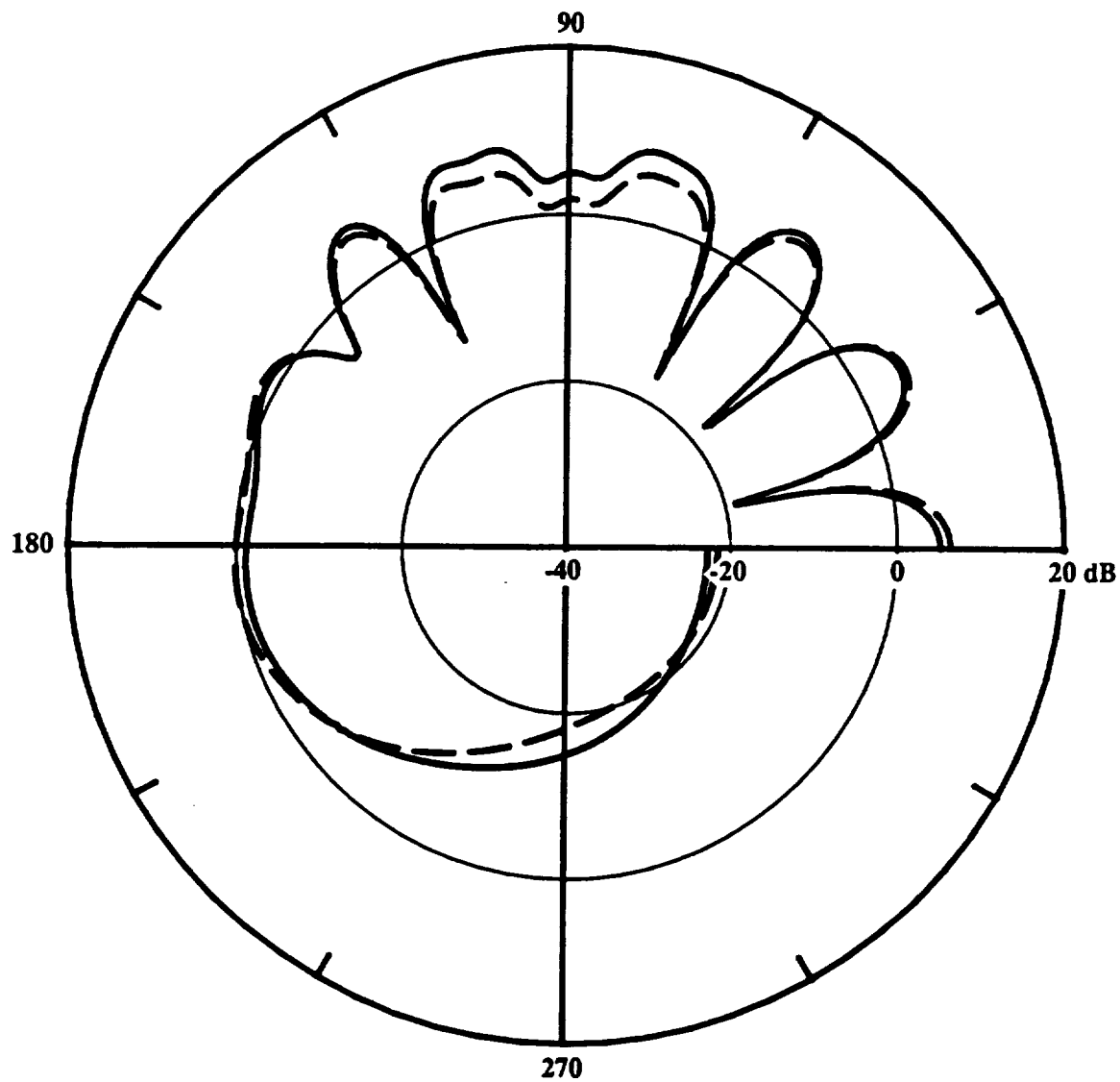


Figure 5b: Normalized directivity of a point source diffracted by a trailing edge in a flow; observer directly above the retarded position of the edge; i.e., $\theta_o = 90$.

$r_i = 1$, $r_o = 1000$, $k_o = 10$, $\theta_i = 38.66$, $M = -0.8$, $\gamma = z_o = 0$.

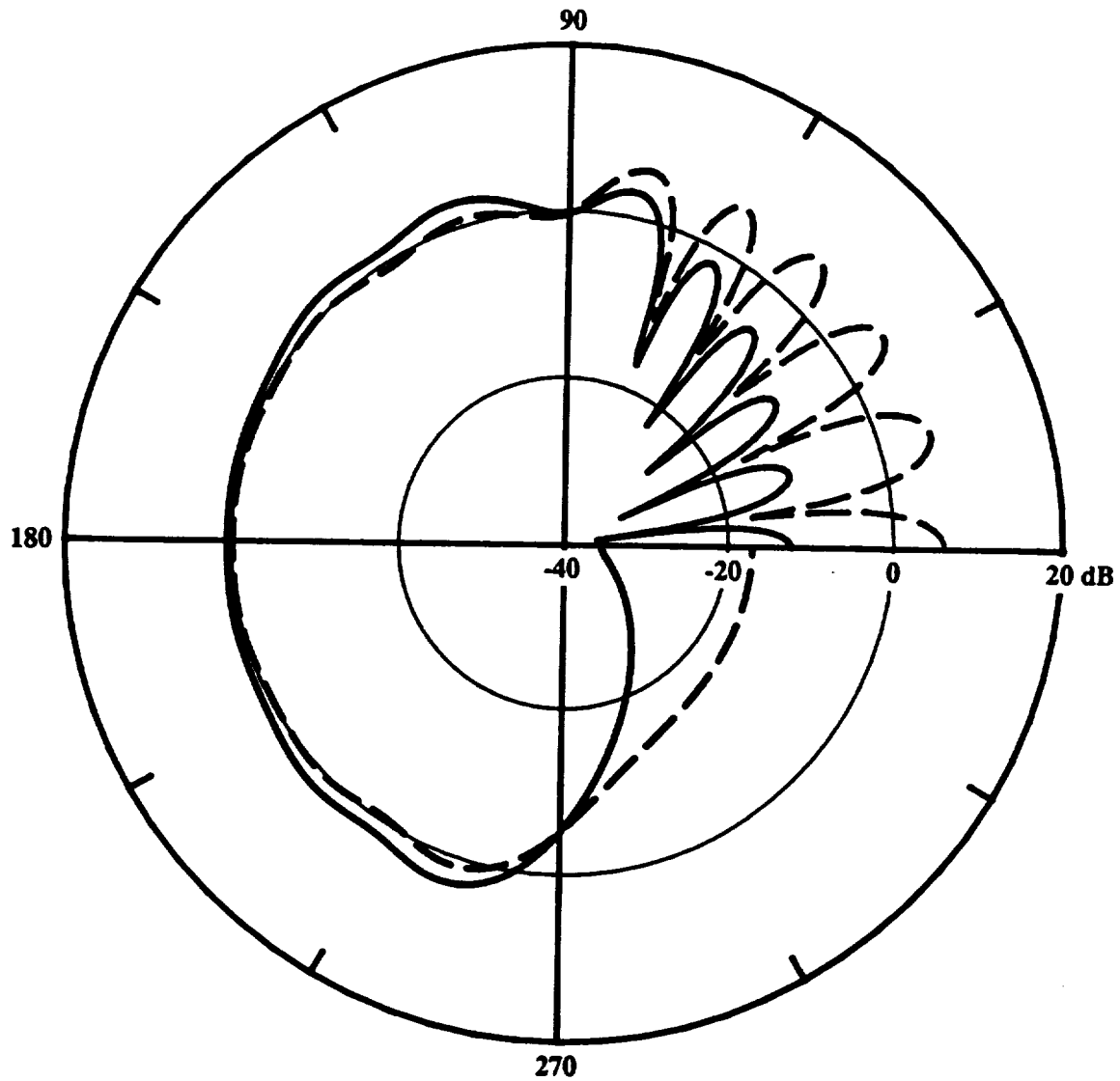


Figure 6a: Normalized directivity of a point source diffracted by a leading edge in a flow; source directly above the present position of the edge.

$r_s = 1$, $r_0 = 1000$, $k_0 = 10$, $\theta_s = 90$, $M = 0.8$, $\gamma = z_0 = 0$.

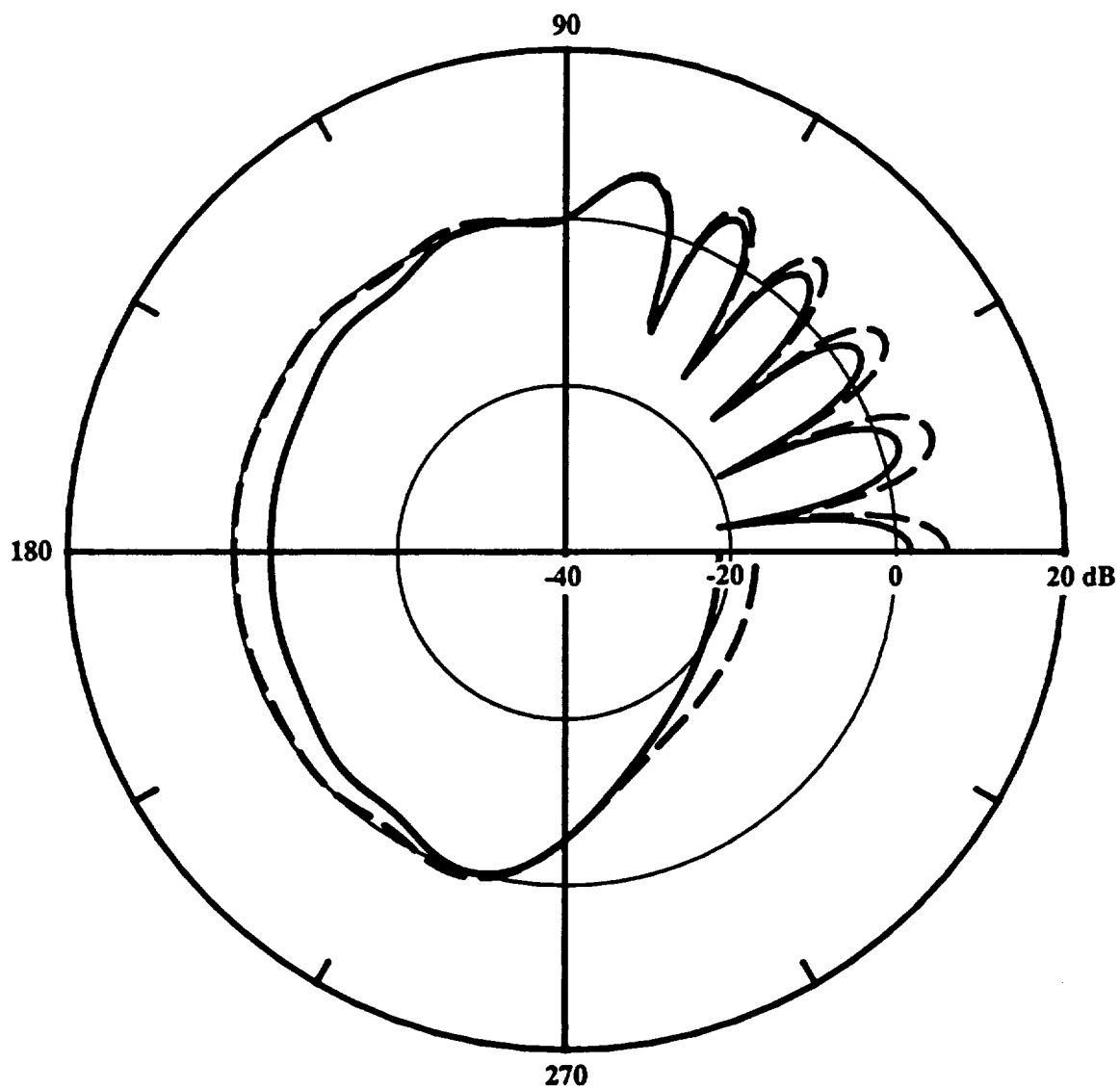


Figure 6b: Normalized directivity of a point source diffracted by a trailing edge in a flow; source directly above the present position of the edge.

$r_s = 1$, $r_o = 1000$, $k_o = 10$, $\theta_s = 90$, $M = -0.8$, $\gamma = z_o = 0$.

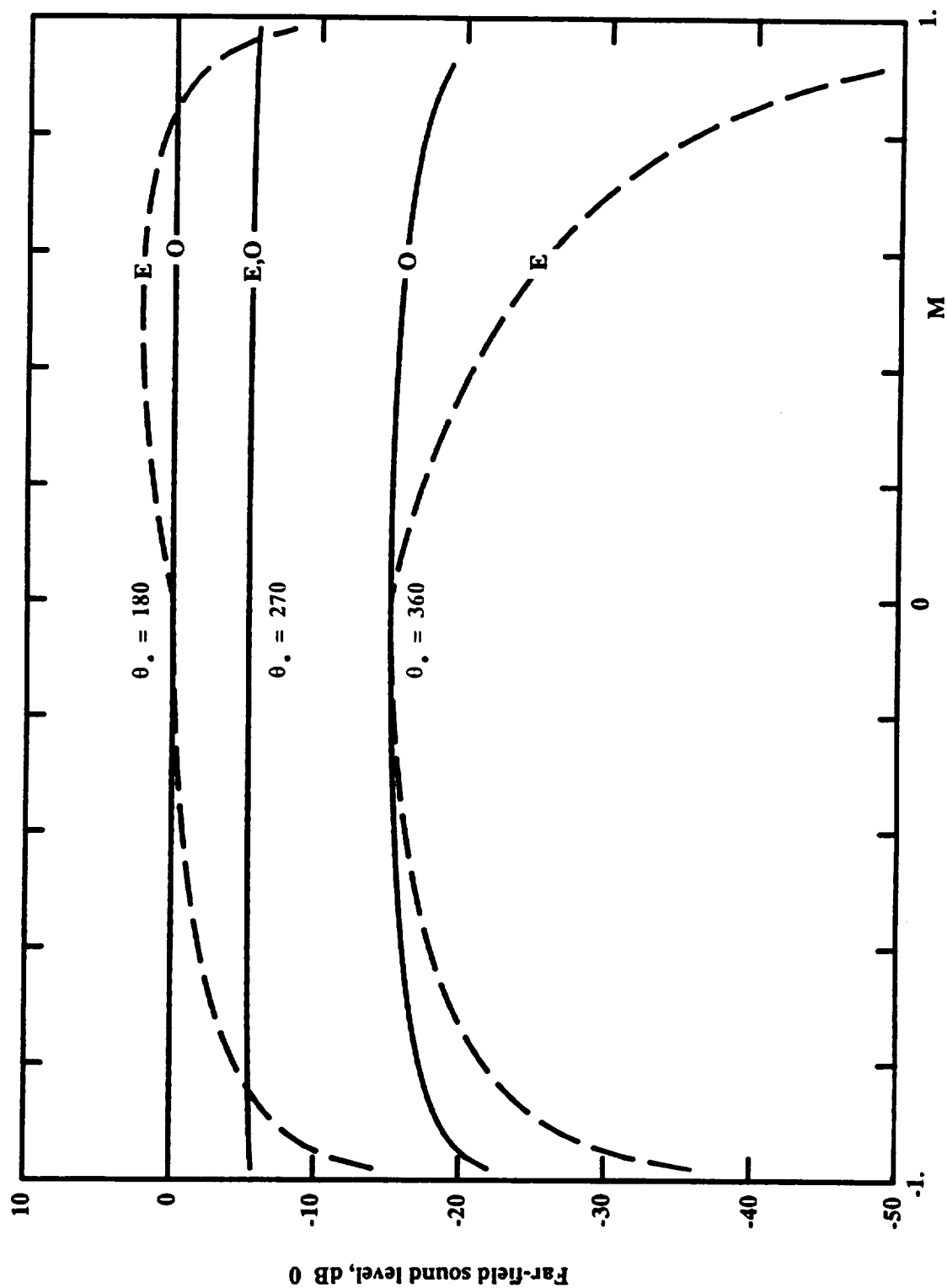


Figure 7a: Mach number effect on diffraction of a point source by an edge for three observer positions, θ_0 .

E \Rightarrow normalized by extrapolated edge pressure; O \Rightarrow normalized by observer pressure without plate. $r_s = 1$, $r_0 = 1000$, $k_0 = 10$, $\theta_s = 90^\circ$, $\gamma = z_0 = 0$.

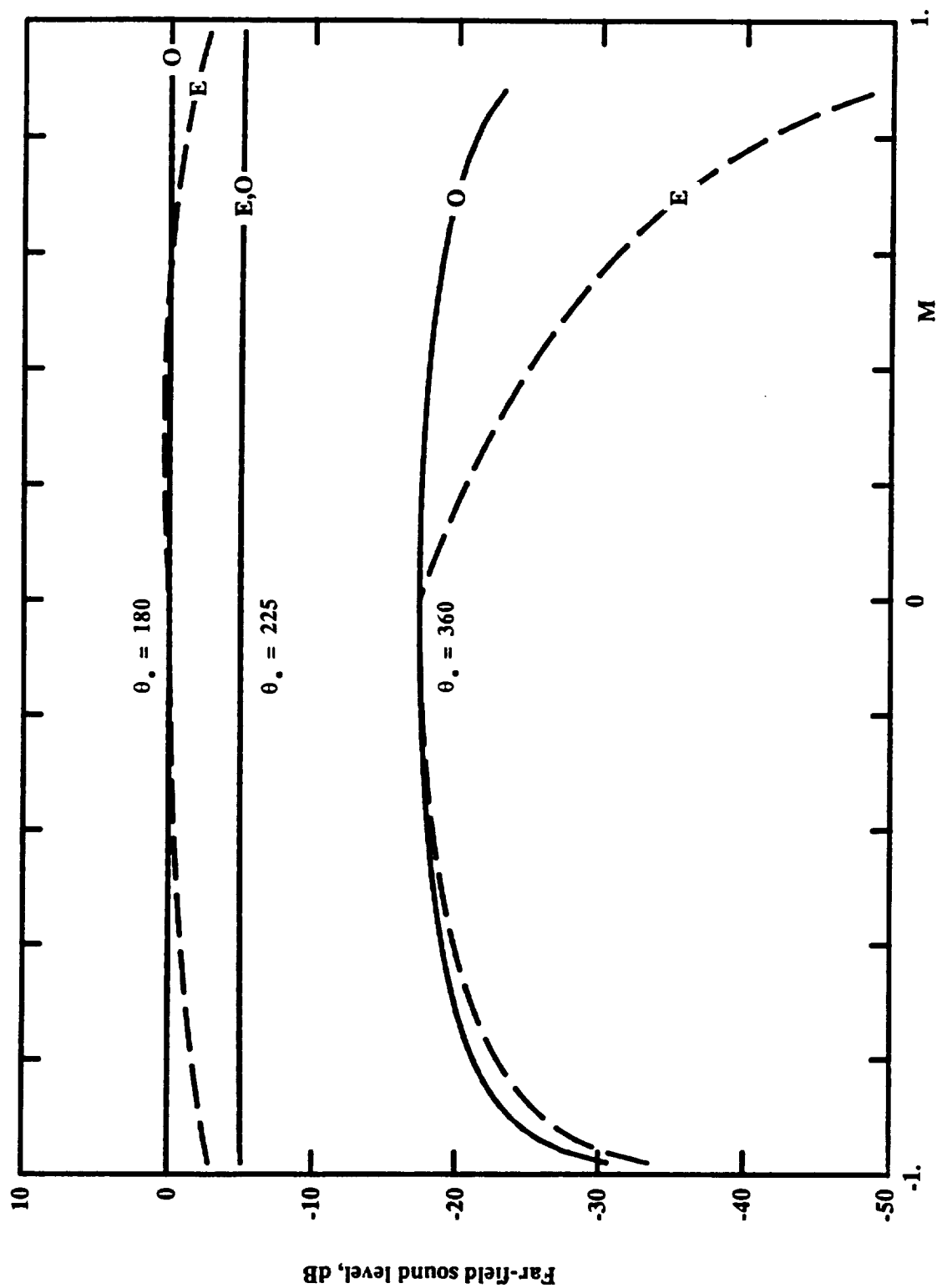


Figure 7b: Mach number effect on diffraction of a point source by an edge for three observer positions, θ_o .
 $E \Rightarrow$ normalized by extrapolated edge pressure; $O \Rightarrow$ normalized by observer pressure without plate. $r_s = 1$, $r_o = 1000$, $k_o = 10$, $\theta_s = 45$, $\gamma = z_o = 0$.

1. Report No. NASA CR 185192		2. Government Accession No.		3. Recipient's Catalog No.											
4. Title and Subtitle Unified Aeroacoustics Analysis for High Speed Turboprop Aerodynamics and Noise. Volume II - Development of Theory for Wing Shielding.				5. Report Date May 1991											
				6. Performing Organization Code											
7. Author(s) R. K. Amiet (Current affiliation: AMI, Wooster, Ohio)				8. Performing Organization Report No. None											
				10. Work Unit No. 535-03-01											
9. Performing Organization Name and Address Hamilton Standard Division United Technologies Corporation PO Box 1000 Windsor Locks, CT 06096				11. Contract or Grant No. NAS3-23720											
				13. Type of Report and Period Covered Contractor Report Final											
12. Sponsoring Agency Name and Address National Aeronautics and Space Administration Lewis Research Center Cleveland, Ohio 44135-3191				14. Sponsoring Agency Code											
15. Supplementary Notes Project Manager, Bruce Clark, Advanced Turboprop Project Office, NASA Lewis Research Center, Cleveland, Ohio 44135															
16. Abstract This report presents a unified theory for aerodynamics and noise of advanced turboprops. Aerodynamic topics include calculation of performance, blade load distribution, and non-uniform wake flow fields. Blade loading can be steady or unsteady due to fixed distortion, counter-rotating wakes, or blade vibration. The aerodynamic theory is based on the pressure potential method and is therefore basically linear. However, non-linear effects associated with finite axial induction and blade vortex flow are included via approximate methods. Acoustic topics include radiation of noise caused by blade thickness, steady loading (including vortex lift), and unsteady loading. Shielding of the fuselage by its boundary layer and the wing are treated in separate analyses that are compatible but not integrated with the aeroacoustic theory for rotating blades. The report is in 5 volumes with titles and contractor report numbers as follows. <table border="0"> <tr> <td>Volume I.</td> <td>"Development of Theory for Blade Loading, Wakes, and Noise", (CR 4329)</td> </tr> <tr> <td>Volume II.</td> <td>"Development of Theory for Wing Shielding", (CR 185192)</td> </tr> <tr> <td>Volume III.</td> <td>"Application of Theory for Blade Loading, Wakes, Noise, and Wing Shielding", (CR 185193)</td> </tr> <tr> <td>Volume IV.</td> <td>"Computer User's Manual for UAAP Turboprop Aeroacoustic Code" (CR 185194)</td> </tr> <tr> <td>Volume V.</td> <td>"Propagation of Propeller Tone Noise Through a Fuselage Boundary Layer", (CR 185195)</td> </tr> </table>						Volume I.	"Development of Theory for Blade Loading, Wakes, and Noise", (CR 4329)	Volume II.	"Development of Theory for Wing Shielding", (CR 185192)	Volume III.	"Application of Theory for Blade Loading, Wakes, Noise, and Wing Shielding", (CR 185193)	Volume IV.	"Computer User's Manual for UAAP Turboprop Aeroacoustic Code" (CR 185194)	Volume V.	"Propagation of Propeller Tone Noise Through a Fuselage Boundary Layer", (CR 185195)
Volume I.	"Development of Theory for Blade Loading, Wakes, and Noise", (CR 4329)														
Volume II.	"Development of Theory for Wing Shielding", (CR 185192)														
Volume III.	"Application of Theory for Blade Loading, Wakes, Noise, and Wing Shielding", (CR 185193)														
Volume IV.	"Computer User's Manual for UAAP Turboprop Aeroacoustic Code" (CR 185194)														
Volume V.	"Propagation of Propeller Tone Noise Through a Fuselage Boundary Layer", (CR 185195)														
17. Key Words (Suggested by Author(s)) Prop-Fan, High Speed Turboprop, Aerodynamics, Noise, Acoustic Shielding, Vortex Lift, Unsteady Lift, Wakes			18. Distribution Statement General release												
19. Security Classif. (of this report) Unclassified		20. Security Classif. (of this page) Unclassified		21. No of pages 37											
				22. Price*											

—

1